ADVANCED MATERIALS
www.advmat.de

Toward Intrinsically Stretchable OLEDs with High Efficiency

*Huanyu Zhou, Hyun-Wook Kim, Woo Jin Jeong, and Tae-Woo Lee**

Wearable electronics require stretchable displays that can withstand large and repeated mechanical deformation without failure. Intrinsically stretchable organic light-emitting diodes (ISOLEDs) that operate under DC voltage provide promising candidates for wearable display applications. However, the lack of sophisticated stretchable materials and processing techniques suitable for ISOLEDs results in a significant deficit in the efficiency of state-of-the-art ISOLEDs compared to industrial standards. The design of stretchable conducting and semiconducting materials poses a significant challenge because of trade-off relationships between stretchability and properties such as conductivity and charge carrier mobility. To increase the efficiency of ISOLEDs to meet industrial standards, strategies to overcome these trade-offs must be developed. This perspective discusses recent progress and challenges in designing stretchable electrodes, light-emitting materials, transport materials, and potential applications of ISOLEDs. It provides a useful guide in this field to develop efficient ISOLEDs for system-level integration.

1. Introduction

Significant advances in materials science and in processing techniques have driven the rapid development of wearable electronics.[1–5] Their designs are evolving from flat and rigid devices to flexible and stretchable ones that can be bent or stretched significantly without breaking (**Figure 1A**).[6–10] Such sensors, affixed to the epidermis of human subjects, can monitor diverse physiological signals that can be projected onto wearable displays (Figure 1B).[11–14] Although these signals can be processed and transmitted to smartphones using Bluetooth, the ultimate objective is to fabricate on-skin displays that can withstand substantial mechanical deformation.[15–18]

Organic light-emitting diodes (OLEDs) have emerged as the leading display technology, due to vacuum processability, high color-rendering index, and superior contrast. OLEDs dominate the current display industry and are poised to enable the realization of durable, highly-efficient wearable displays. Currently, two approaches are being pursued to achieve stretchability: creating geometrically-stretchable structures and developing intrinsically stretchable materials that can withstand mechanical deformation.[19,20]

Geometrically stretchable structures are typically fabricated through complex processes. One widely-used method employs out-of-plane buckling structures; this process, OLEDs and ultrathin substrates are applied to a pre-strained elastomer.[21] When the stress is released, the elastomer contracts, developing periodic wrinklesthat provides stretchability.[22] Another strategy involves depositing OLEDs onto regions of soft elastomers, which have been toughened by photo-crosslinking to limit the strain experienced by the device.[12] However, the materials used in these devices are not intrinsically stretchable and may degrade when subjected to unexpected mechanical deformation.

The use of intrinsically stretchable organic light-emitting diodes (ISOLEDs) may provide a solution to this problem. ISOLEDs are composed of stretchable materials that can endure significant mechanical deformation while maintaining functionality. They also feature less-complex architecture than conventional OLEDs, which include charge injection, transport, blocking, and light-emitting layers. The simplicity of ISOLEDs can be attributed to the lack of stretchable materials and difficulties in vertically stacking multiple stretchable materials using solution processes.

Improvements of light-emitting materials have led to a significant increase in the external quantum efficiency (EQE) of conventional OLEDs to 40%, but ISOLEDs have yet to reach comparable efficiency (**Figure 2**).[23] Despite recent advances in stretchable materials, the highest current efficiency (CE) achieved by ISOLEDs is 20.3 cd A^{-1}, which is substantially lower than that of state-of-the-art rigid OLEDs.[24]

The challenge in improving the efficiency of ISOLEDs lies in overcoming the inherent trade-off relationships between the mechanical and electronic properties of intrinsically stretchable

H. Zhou, H.-W. Kim, W. J. Jeong, T.-W. Lee
Department of Materials Science and Engineering
Seoul National University
Seoul08826, Republic of Korea
E-mail: twlees@snu.ac.kr

H. Zhou
BK21 PLUS SNU Materials Division for Educating Creative Global Leaders
Seoul National University
Seoul08826, Republic of Korea

T.-W. Lee
Institute of Engineering Research
Interdisciplinary Program in Bioengineering
Research Institute of Advanced Materials
Soft Foundry
Seoul National University
Seoul08826, Republic of Korea

T.-W. Lee
SN Display Co., Ltd.
Seoul 08826, Republic of Korea

The ORCID identification number(s) for the author(s) of this article can be found under https://doi.org/10.1002/adma.202420008

DOI: 10.1002/adma.202420008

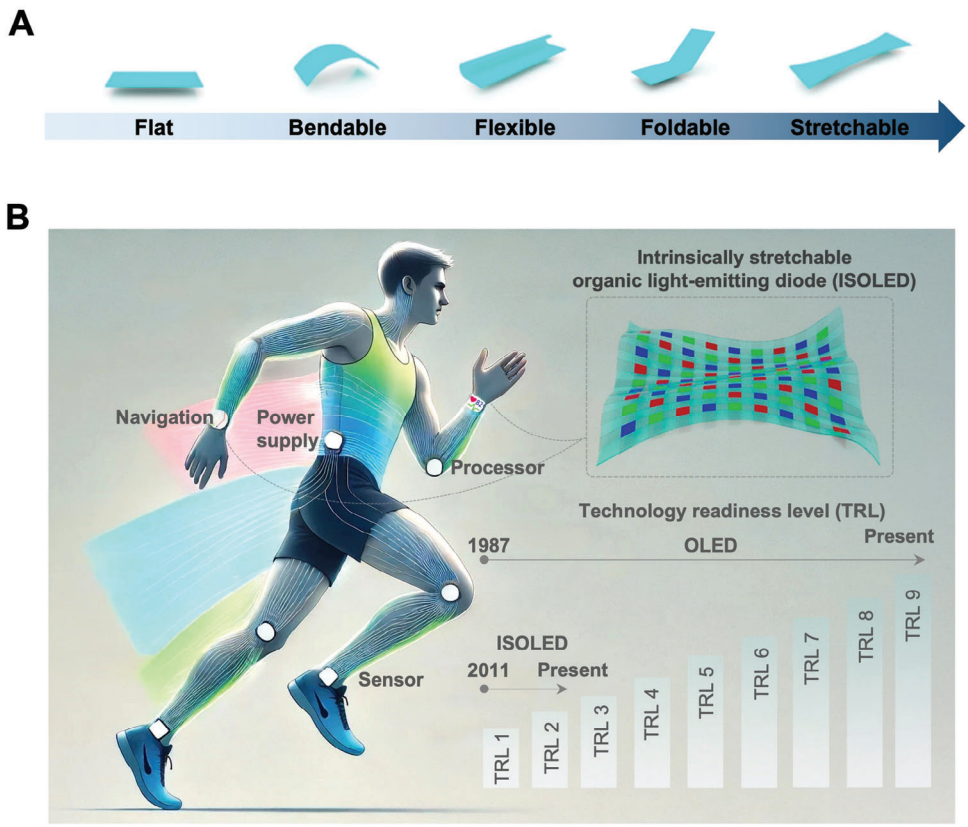

Figure 1. A) Evolution of display form factors, from the conventional flat organic light-emitting diodes (OLEDs) to intrinsically stretchable organic light-emitting diodes (ISOLEDs). B) Schematic illustration of wearable displays attached to human skin, visualizing various wearable sensor signals (left) and providing navigation information (right). Comparison of the technology readiness level of conventional OLEDs and ISOLEDs.

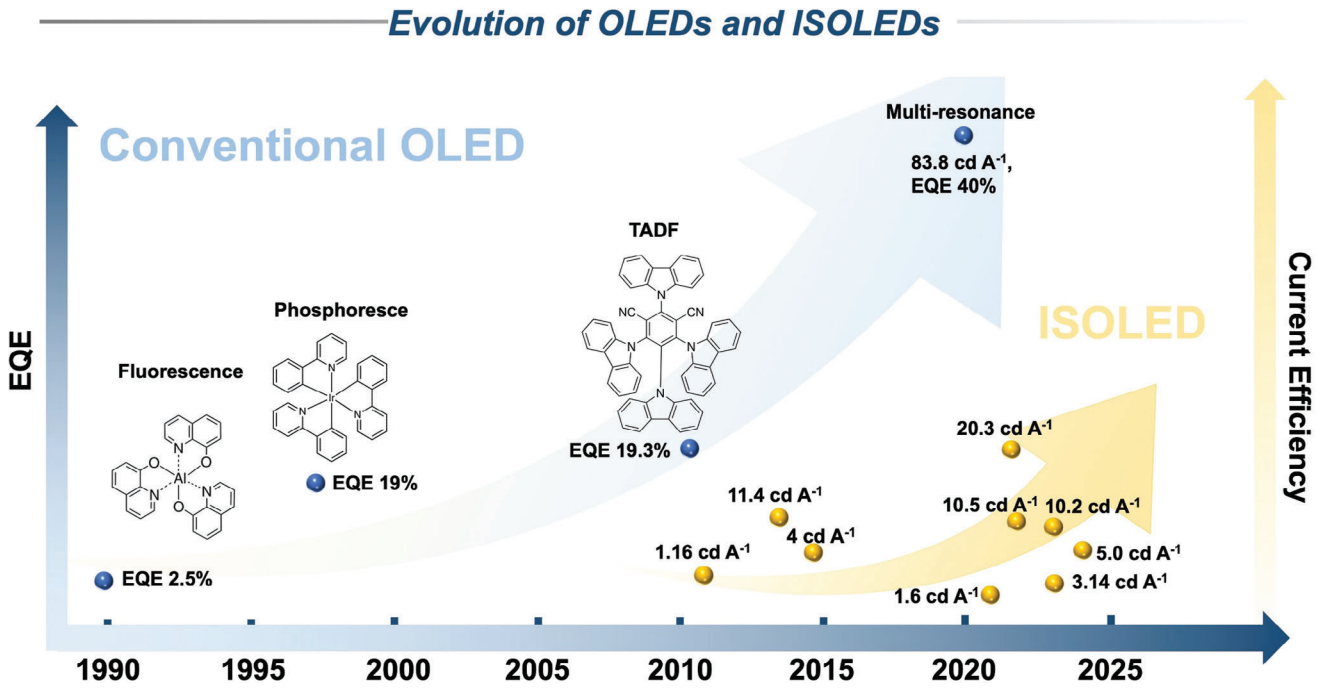

Figure 2. Evolution of external quantum efficiency (EQE) and current efficiency of OLEDs and ISOLEDs. The large efficiency gap between ISOLEDs and OLEDs highlights the need for further significant efforts to minimize this gap and achieve comparable efficiency. Data for conventional OLED are from references;[23,86–88] data for ISOLEDs are listed in Table 2.

materials. For example, conductivity is primarily governed by the percolation threshold;an increase in filler content results in increased conductivity.[25] However, when the elastomer content is insufficient, most of the strain energy is absorbed by the conductive fillers rather than by the elastomer matrix, so stretching yields mechanical failure. Conversely, when the elastomer content is insufficient, most of the strain energy is absorbed by the conductive fillers rather than by the elastomer matrix, leading to mechanical failure when stretched. Stretchable semiconducting materials also show these trade-offs between mechanical stretchability and electronic properties. Increasing the elastomer content or inserting flexible spacers as an alternative method to enhance stretchability inevitably disrupts the conjugated structure and degrades the material's electronic properties.[26]

Herein, we provide an overview of recent advances in stretchable materials for ISOLEDs, including stretchable electrodes, light-emitting materials, and charge-injection/transport materials. The mechanical and electrical properties of these materials, along with the processing techniques used for the fabrication of ISOLEDs, strongly influence their stretchability and on the electrical characteristics of the devices. We will discuss how these properties can be optimized to achieve ISOLEDs that are simultaneously highly efficient and stretchable. We will also highlight potential applications of ISOLEDs, such as in flexible and wearable displays, and discuss the challenges that must be overcome to realize the full potential of ISOLEDs in these applications. By presenting a comprehensive understanding of the design principles and potential applications of ISOLEDs, this perspective aims to provide a useful guide in this field to develop highly-efficient stretchable displays for wearable applications.

2. Comparison of OLEDs with Other Stretchable Light-Emitting Devices

Alternating-current electroluminescence (ACEL) devices apply a unique approach to achieving light emission using inorganic phosphors to generate field-driven electroluminescence. These devices have the simplest structure: a stretchable light-emitting layer, typically composed of a dielectric material and a phosphor like ZnS:Cu, sandwiched between two stretchable electrodes (**Figure** 3A). Without direct charge injection into the active layer, ACEL devices require low conductivity in their stretchable electrodes, which allows them to achieve high stretchability as much as several hundred percent without compromising electrical characteristics.

In contrast, light-emitting electrochemical cells (LECs), which incorporate electrolytes directly in the light-emitting layer, can operate under both forward and reverse bias conditions. LECs may exhibt slight turn-on voltage variations due to barriers to ion mobility and to charge injection; however, this design facilitates efficient bipolar operation. LEC also features a straightforward sandwich structure, where the light-emitting material is mixed directly with electrolytes (Figure 3B). The stretchability of LECs mainly derives from the viscoelasticity of these electrolytes, which gives them moderate stretchability, which is lower than that of ACEL devices but with the advantage of a very low turn-on voltage due to the presence of the electrolytes.

Finally, OLEDs possess the most complex and intricate structure among these devices, incorporating multiple functional layers dedicated to increasing efficiency (Figure 3C). Light-emitting diodes are primarily classified by the type of light-emitting material; types include OLEDs, quantum dot light-emitting diodes (QLEDs), and perovskite light-emitting diodes (PeLEDs). Among them, OLEDs, which have already been commercialized, have the highest efficiency, longest device-operation lifetime, and greatest scalability.

At the threshold voltage, all of these types of light-emitting diodes undergo a sharp current increase, which is a characteristic of diode behavior. However, the inherent rigidity of pure inorganic quantum dots and perovskites restricts their use in stretchable applications. To date, most stretchable light-emitting devices utilize organic materials, which have the advantages of solution processability and inherent stretchability. Nevertheless, this complexity of device structure often limits their stretchability compared to ACEL and LEC devices.

The structural design of these stretchable light-emitting devices is linked to their operating mechanisms. In ACEL devices, light emission arises from impact excitation, wherein hot electrons directly collide with localized luminescent centers. This process requires a high electric field, typically $> 10^6$ V cm^{-1} (Figure 3D).[27] Thus, enhancing increasing the electric field experienced by the phosphor, is crucial for improving luminescent properties. This increase can be achieved either by raising the applied voltage or by increasing the dielectric constant of the stretchable light-emitting layer. In contrast, LECs operate by electrolyte dissociation, with ions drifting toward opposite electrodes to establish interfacial dipole regions. This dipole significantly bends the energy bands, and thereby facilitates charge injection by tunneling (Figure 3E). This unique mechanism enables efficient charge injection across barriers, and requires a minimal number of functional layers. However, LECs have limited electrochemical stability under long-term operation.

For OLEDs, efficient light emission depends on charge injection from the electrodes into the light-emitting layer. This process is primarily governed by the charge-injection barrier at the interfaces between electrodes and organic materials (Figure 3F). Reducing this barrier and increasing interface quality are critical for improving OLED efficiency. However, creating ISOLEDs remains challenging due to the need to design multiple stretchable materials (e.g., hole/electron injection and transport layers, light-emitting materials, and compliant anodes and cathodes), and to vertically stack them to form a stretchable device.

3. Intrinsically Stretchable Transparent Conductive Electrodes

Mechanical bending strain is proportional to substrate thickness; thus, conventional devices fabricated on rigid substrates composed of metals or ceramics can be made flexible by reducing their thickness.[28,29] With sufficiently small thickness, Si, which has Young's modulus Y on the gigapascal scale, could also become flexible. However, such materials and devices are intrinsically rigid,[30,31] and cannot sustain extreme mechanical deformation such as stretching or twisting that occurs in practical wearable applications. Human skin has~ 57 MPa $\leq Y \leq \sim$ 140 MPa at a maximum tensile strain ε_{max} of 60%.[32] To prevent mechanical failure due to mismatches in mechanical properties, materials and devices designed for skin attachment should ideally have a Y

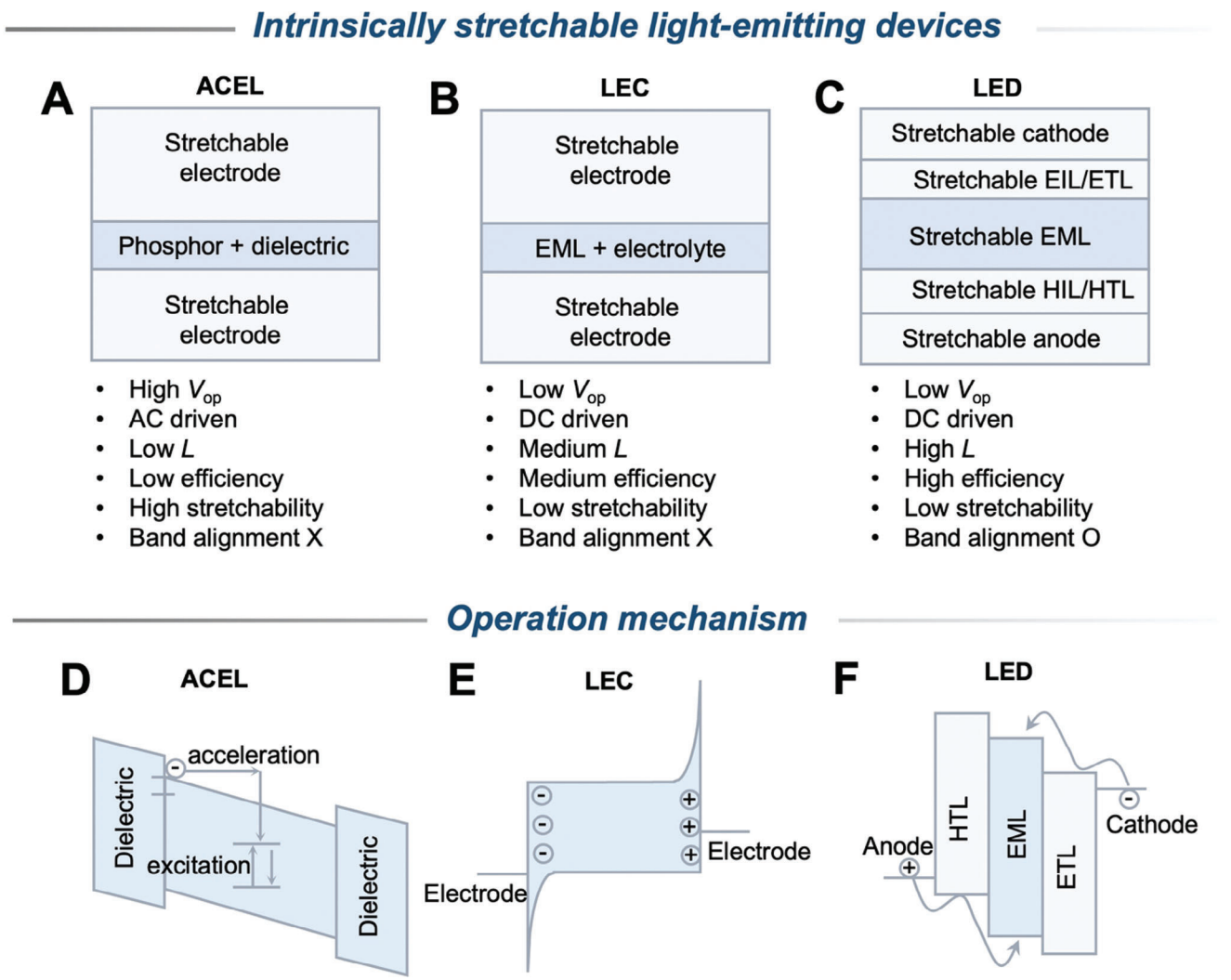

Figure 3. Comparison of device architecture and characteristics of different ISOLEDs: A) alternating-current electroluminescence (ACEL), B) light-emitting electrochemical cell (LEC), and C) light-emitting diode (LED). Comparison of operation mechanisms of D) ACEL, E) LEC, and F) LED. HTL (hole transport layer); EML (light-emitting layer); ETL (electron transport layer).

within or lower than this range and be capable of sustaining ε_{max} > 60% to ensure mechanical reliability.

When designing intrinsically stretchable conductors for wearable applications, conductive fillers such as liquid metal, 1D, 2D, or conducting polymers are incorporated with rubber-like elastomers to lower the Y of the stretchable conductors and to attain stretchability (**Figure** 4A). With high electrical conductivity and high stretchability, stretchable conductors that are obtained using blending methods can be applied for wearable or implantable sensors, circuits, and other logic units. However, for use of ISOLEDs in such applications, such stretchable conductors must have high optical transmittance (T, typically measured at 550 nm) to ensure efficient light extraction through the stretchable transparent conductive electrodes (TCEs) (**Table 1**).[4] Stretchable conductors prepared using the blending method have reached ε_{max} > 500%, but they contain a large volume fraction of conductive fillers and therefore have insufficient T, which limits their applications as TCEs.

The charge-injection properties of the stretchable TCEs are also important in ISOLEDs. Charge injection from both the anode and cathode to the light-emitting layer determines the efficiency of the ISOLED. Efficient hole injection requires an anode that has high work function (WF) > 4.8 eV, and efficient electron injection requires a cathode that has a low WF < 4.0 eV. Hence, simultaneously achieving high stretchability, high conductivity, high transparency, and high efficiency of carrier injection remains challenging in the field of stretchable TCEs. Here we consider three classes of materials that are added to stretchable TCEs to increase their T, sheet resistance R_s, and ε_{max}: metal nanowires, carbon-derived 1D and 2D materials, and conducting polymers (Figure 4B).

Metal nanowires such as silver nanowires (AgNWs) have been the most widely used conductive filler for ISOLED fabrication. Due to the high aspect ratio of AgNWs, the percolation threshold of AgNWs is one to two orders of magnitude lower than that of spherical nanoparticles, so high conductivity can be achieved

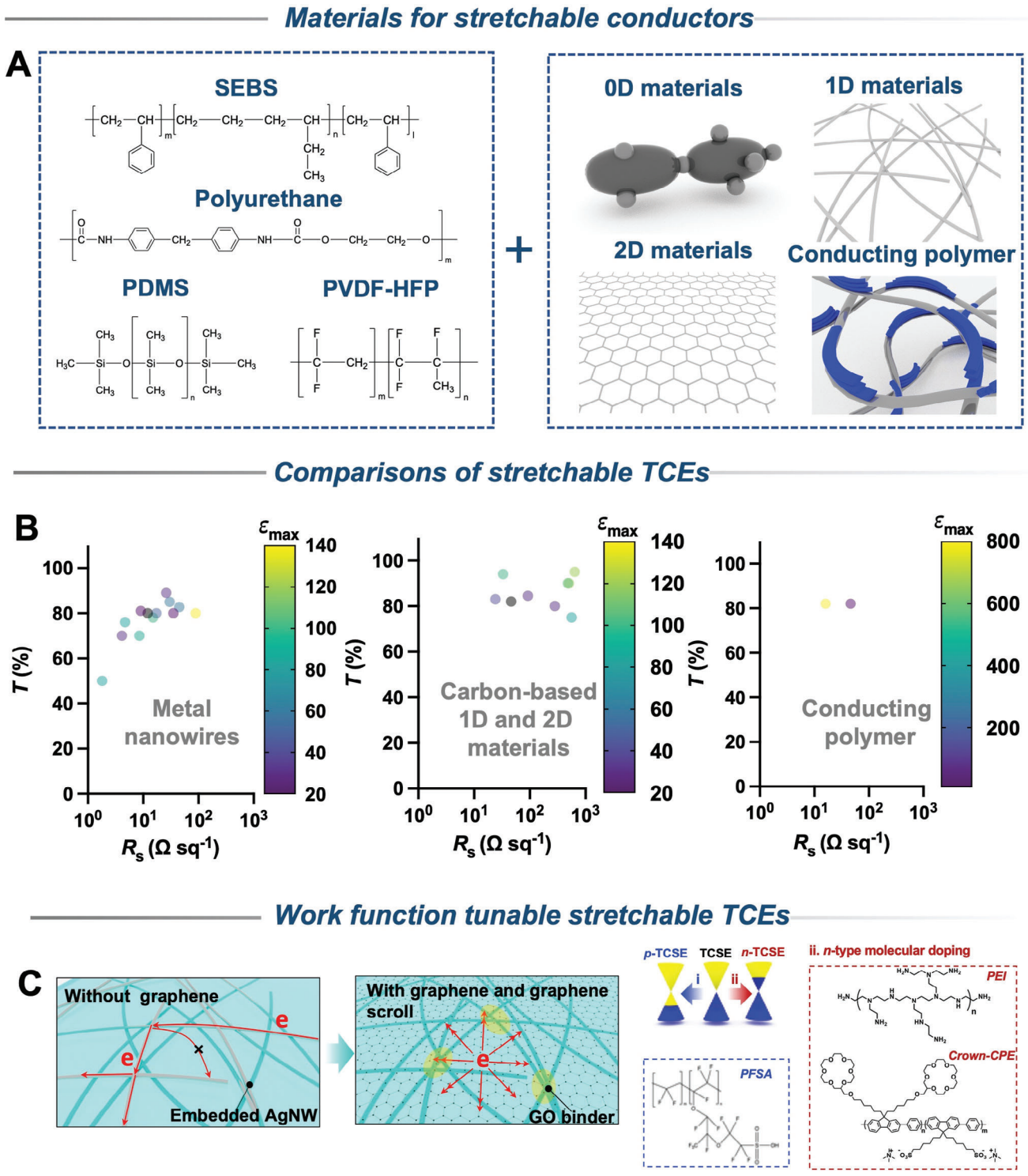

Figure 4. Strategies to achieve intrinsically stretchable electrodes for display applications. A) Combining elastomers as the polymer matrix, and conducting nanomaterials and polymer as the fillers for stretchable conductors. B) Comparison of optical transparency T, sheet resistance R_S, and maximum tensile strain ε_{max} of stretchable transparent conductive electrode (TCEs) metal nanowires, carbon-derived 1D and 2D materials, and conducting polymers. C) Schematic illustration of the graphene-derived WF tunable stretchable TCEs that use perflurosulfonic acid (PFSA) as the p-type dopant, and polyethyleneimine (PEI) and crown conjugated polyelectrolyte (Crown-CPE) as the n-type dopant, to overcome the charge-injection limitations of silver nanowires. Reproduced with permission.[24] Copyright 2022, WILEY-VCH.

Table 1. Comparison of State-of-the-Art Stretchable Transparent Conductive Electrodes for ISOLEDs.

Material type	Compositions	Transmittance @ 550 nm [%]	Sheet resistance [Ω sq^{-1}]	Resistance change (specific tensile strain)	Work function [eV]
1D	AgNW/GO/PUA[37]	88	14	3.2 (ε = 40%)	–
	AgNW/polyacrylate[89]	87.5	17.2	2.3 (ε = 50%)	–
	AgNW/aerogel/PDMS[90]	87	500	1.45 (ε = 40%)	–
	ZnO/PEIE/AgNW/PEIE/ZnO[53]	85	40	11 (ε = 40%)	–
	AgNW/CF/PDMS[91]	85	15	15 (ε = 40%)	
1D/2D	AgNW/GO/Graphene/[24]	88	24	3.9 (ε = 40%)	3.63-5.69
	CP-AgNW/GO/Graphene[35]	–	21	1.81 (ε = 40%)	–
Polymer	PEDOT:PSS:FS30[54]	–	–	–	4.73-5.35

without compromising T.[33] AgNW percolation networks are embedded on the surface of the elastomer, which effectively reduces the surface roughness, compared to coating AgNWs on the surface of the substrate.[34] Small protrusions or high surface roughness R_{rms} in stretchable TCEs causes high leakage current and catastrophic failure, especially at high voltage.[35] Cold pressing the surface of AgNW networks before the embedding process decreases R_{rms} of the electrode, decreases the number of protrusions, and significantly reduces leakage current.[35]

Increasing ε_{max} of stretchable TCEs that use AgNWs increases the endurance of the ISOLED to external tensile strain. The interaction between the elastomer matrix and AgNWs is critical for strain energy dissipation. The Hansen solution parameter effectively estimates the miscibility between the elastomer matrix and the polyvinylpyrrolidone (PVP) ligand that wraps the surface of AgNWs. The miscibility increases with decreasing distance R in Hansen space,[14]

$$R = \left[\left(\delta_{D1} - \delta_{D2}\right)^2 + 0.25\left(\delta_{P1} - \delta_{P2}\right)^2 + 0.25\left(\delta_{H1} - \delta_{H2}\right)^2\right]^{1/2} \quad (1)$$

where δ_{Di} (i = 1, 2 are the species) indicates dispersion force, δ_{Pi} indicates dipole intermolecular force, and δ_{Hi} indicates to hydrogen bonds. The estimation shows that PVP ligand mixes better with styrene-ethylene-butadiene-styrene (SEBS) than with the widely-used poly(dimethylsiloxane) (PDMS).[24] Furthermore, a copolymer of urethane acrylate and dimethyl acrylate also shows good interaction with AgNWs and excellent mechanical stretchability.[36] The sheet resistance R_s of embedded AgNWs remains unchanged even after 100-time peeled-off test; this result proves the good adhesion between the elastomer matrix and the PVP ligand and facilitates uniform strain energy dissipation under stretching.

To further increase the stretchability of the AgNWs, the interaction between AgNWs at the junction is also important. Under large deformation, twisting, disjointing, and sliding of AgNWs at the junction degrade the electrical conductivity, so junction welding is important for stretchable TCEs. Graphene oxide (GO) with abundant oxygen-containing groups can wrap the AgNW junctions, reduce the junction resistance, and increase the stretchability of the electrodes.[37] The stretchability of AgNW percolation networks originates from the fishnet model, in which AgNW networks deform under strain while the junction remains in electrical contact due to the GO welding. However, complete welding of AgNW junctions limits the deformation tolerance and increases the stiffness of AgNW networks.[36] Therefore, to balance the stretchability and electrical conductivity of AgNW networks, the welding conditions must be optimized.

Metallic carbon nanotubes (CNTs) have extremely high $1 \leq Y \leq 5$ TPa, so they offer an opportunity to increase the stretchability of the electrode.[38] CNTs have low conductivity of ≈ 100 S cm^{-1} and poor solubility in solvents, therefore, their applicability for use in stretchable TCEs is limited.[38] To achieve a CNT electrode that has R_s comparable to that of conventional ITO electrodes the concentration of CNTs must be high, which significantly decreases the T of the electrode, so the opaque CNT electrode is favorable only for stretchable circuits and sensor applications that do not require high T.[39] Thus, chemical modification of the CNTs surface to simultaneously achieve high T and high electrical conductivity is an open problem.

Conducting polymer poly(3,4-ethylenedioxythiophene):polystyrene sulfonate (PEDOT:PSS) is another promising candidate for use in stretchable TCEs. However, pristine PEDOT:PSS has a high $Y > 2$ GPa, which results in a large mismatch between the Y of the polymer film and of the elastomer substrate.[40,41] The crack-onset strain of pristine PEDOT:PSS is as low as 5%. Post-treatments using polar solvents or acids remove excess PSS, and induces a change from the coiled benzoid to planar quinoid structure, and thereby significantly increases electrical conductivity from 1 to > 1000 S cm^{-1}. However, these changes decrease the stretchability due to the removal of the soft PSS matrix. The key to improving the stretchability of the PEDOT:PSS without sacrificing its conductivity and T is to induce a phase separation between PEDOT and PSS and form a 1D nanofibril structure using ionic additives.[42] The charge screening effect of such water-soluble ionic additives facilitates the morphological change from a planar to an interconnected PEDOT nanofibril structure which is embedded in the soft PSS domains.[43] The resultant film has high conductivity of 3100 S cm^{-1} at ε = 0%, and ε_{max} = 800%.

Despite the significant improvement in electrical conductivity and stretchability of stretchable TCEs, a remaining challenge is their poor charge injection capability, which primarily depends on the electrical contact area and the charge injection barrier. AgNW percolation networks are surface-embedded with only half of the surface exposed to air; this condition significantly reduces the electrical contact area between AgNWs and the adjacent organic layers. WF tunability of current stretchable TCEs is limited from the material point of view. The AgNWs are wrapped by

PVP ligands, so the WF of AgNW cannot easily be tuned. Furthermore, PEDOT:PSS is a p-type conducting polymer, so it is unfavorable for efficient electron injection.

Solving the charge-injection problem at the interface between stretchable TCEs and the organic material may largely mitigate the relative inefficiency of ISOLEDs compared to conventional OLEDs. As one attempt to solve this problem, graphene and graphene scrolls have been introduced to surface-stretchable TCEs to form a 2D contact stretchable electrode. The graphene layer increases the electrical contact area, and can modify the WF to as low as 3.57 eV and as high as 5.69 eV, thereby improving both the electron and hole injection capabilities of the TCEs (Figure 4C).[24] Graphene scrolls help maintain the conduction path during stretching, and GO binder effectively welds the interfaces between AgNW/AgNW and AgNW/graphene. Thus, the mechanical stretchability was not decreased even with the inclusion of 2D materials. Fine-tuning of the WF achieved a current efficiency of 20.3 cd A^{-1}, which is the record high among ISOLEDs.

Further development of ISOLEDs requires the design of suitable stretchable TCE materials; and this is a challenging task that demands simultaneous consideration of parameters such as stretchability, electrical conductivity, *T*, and charge-injection capability. Development of new electrode materials and strategies must consider these trade-off relationships.

4. Intrinsically Stretchable Hole Injection/Transport Materials

Conventional OLEDs consist of multiple layers that are designed to ensure efficient charge injection and transport into the light-emitting layer (EML), and to achieve an optimal charge balance. Holes injected from the anode pass through a hole injection layer (HIL) and a hole transport layer (HTL) before reaching the EML, where they must be balanced by electrons that enter through the electron injection layer (EIL) and electron transport layer (ETL). This balance is crucial for enhancing device efficiency and extending operational lifetime.[44]

Without these layers, charge carriers must surmount substantial energy barriers (i.e., electron injection and hole injection barriers) to reach the EML. These barriers arise due to an energy mismatch between the electrode WF and the EML energy levels. For efficient electron injection, the electron affinity (EA) of the EML should ideally be larger than the WF of the cathode (WF_c), whereas for effective hole injection, the ionization potential (IP) of the EML should be smaller than the WF of the anode (WF_a). Commonly used materials, such as aluminum (cathode; WF_c = 4.3 eV) and indium tin oxide (ITO, anode; WF_a = 4.8 eV), present significant charge injection barriers when paired with commercially used materials like the green OLED emitter $Ir(ppy)_2acac$ (EA = 3.0 eV, IP = 5.5 eV).[45] The hole injection barrier can be defined as

$$\Delta E_e = WF_c - EA \quad (2)$$

and the electron injection barrier as

$$\Delta E_h = IP - WF_a \quad (3)$$

These barriers can be reduced by tuning the electrode Fermi level and achieving Ohmic contact between electrodes and the EML; to maximize OLED efficiency, these adjustments are essential. Hole injection enhancements can be accomplished using hole-transport materials, typically conjugated organic molecules with high WFand high hole mobility (**Figure 5A**). However, because organic semiconductors generally have low conductivity, the Ohmic resistance of the transport layer raises the device's operating voltage above the built-in voltage.[46] To minimize these Ohmic losses, HTLs often require additional doping with p-type dopants, commonly referred to as hole injection materials.[47] This doping effectively increases charge carrier density, and thereby decreasing the operational voltages and improving device efficiency.

In p-type doping, dopants extract electrons from the highest occupied molecular orbital (HOMO) level of semiconductors; this process generates holes.[48] Inorganic compounds like metal oxides are particularly effective as p-type dopants. For example, MoO_3, which has a high EA = 6.8 eV and a low-lying HOMO, is widely used as a HIL material that p-dopes semiconducting transport layers effectively.[49] High carrier mobility and chemical stability of MoO_3 further increase its suitability as a p-type dopant. However, it is inherently brittle and requires high-temperature annealing;[50] these traits limit its applicability in solution-processed ISOLEDs, which must be flexible and amenable to fabrication using low-temperature processes.

Developing hole-injection materials for ISOLEDs is particularly challenging, as these materials need to combine tunable WF, high hole mobility, and mechanical deformability. Typically, these materials are composed of soft polymers or elastomer blends, which are well-suited to solution processing. PEDOT:PSS is a promising HIL candidate that meets these requirements.

The conjugated $PEDOT^+$ component serves as a p-type polymer with high hole mobility (Figure 5B). The positive charges on $PEDOT^+$ are balanced by Coulombic interactions with negatively charged, water-soluble PSS^-, enabling it to remain stably dispersed in aqueous solutions. Due to the high ionization energy of PSS^-, PEDOT:PSS has $5.0 \leq WF \leq 5.2$ eV,[51] which facilitates effective hole injection into the EML by forming an Ohmic contact. Furthermore, the mechanical properties of PEDOT:PSS can be tuned to enhance stretchability, making it an attractive HIL material for ISOLED applications.

For ISOLED applications, PEDOT:PSS must endure considerable strain without forming cracks. However, pristine PEDOT:PSS has limited stretchability, with a crack-onset strain typically < 10%,[52] so for use in ISOLEDs, its stretchability must be increased. Various strategies have been explored to increase itsstretchability, primarily by incorporating soft polymeric additives or by enlarging the PSS^- domain within the blend. The proportion of soft PSS^- significantly influences the mechanical properties of the blend. Reducing the electrostatic interactions between $PEDOT^+$ and PSS^-, and thereby inducing phase separation between them, has effectively increased stretchability.[4,42]

Surfactants and ionic species are commonly used additives that effectively screen electrostatic interactions and modify PEDOT:PSS morphology. In its pristine form, PEDOT:PSS has a granular structure, with water-soluble PSS^- surrounding hydrophobic $PEDOT^+$ in an aqueous medium.[42] Charge-screening additives enlarge the PSS^-

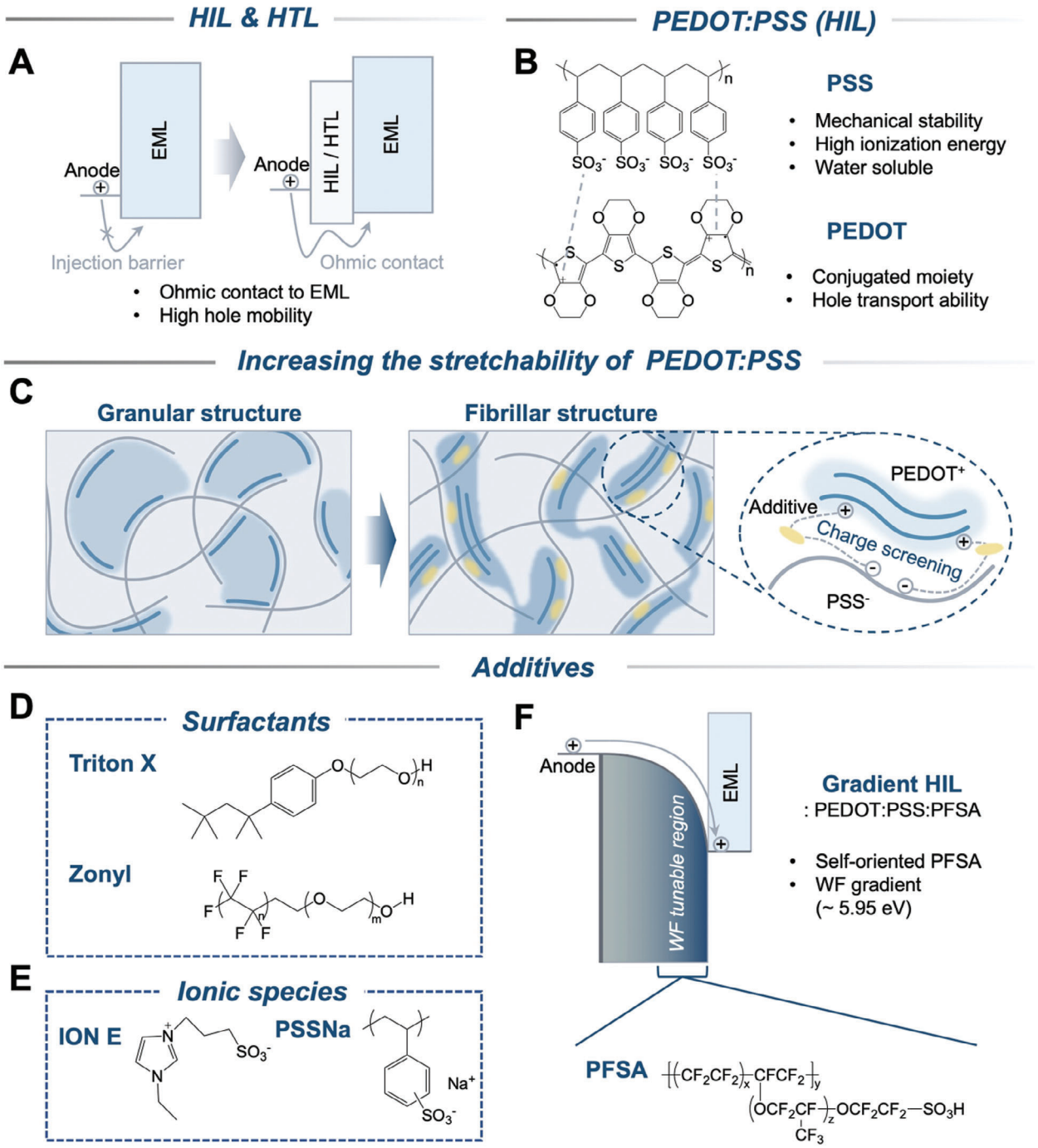

Figure 5. A) Schematic illustration of the energy band structure with and without hole injection layer (HIL)/hole transport layer (HTL). B) Chemical structure of PEDOT:PSS. C) Schematic illustration of stretchability enhancement mechanism of PEDOT:PSS. Chemical structures of representative D) surfactants, and E) ionic species used as additives to increase PEDOT:PSS stretchability. F) Energy band diagram of gradient HIL with addition of PFSA.

domains, thus transforming this morphology to a fibrillar structure, which significantly increases stretchability (Figure 5C). Surfactants, which consist of hydrophilic heads and hydrophobic tails, are especially effective for increasing PEDOT:PSS stretchability (Figure 5D). The hydrophilic head interacts with PSS^-, while the hydrophobic tail interacts with $PEDOT^+$; these complementary interactions facilitate phase separation, which reduces Y from 100 to 2.5 MPa, and enables strain tolerance up to 160% without crack formation.[53]

Ionic species are also highly effective in increasing the stretchability of PEDOT:PSS, either by promoting phase separation between $PEDOT^+$ and PSS^- or by their intrinsic softness reducing the blend's Y (Figure 5E). Their strong charge-screening ability

allows counter-ions to neutralize the charges on $PEDOT^+$ and PSS^-, thereby disrupting electrostatic interactions and promoting a more-flexible morphology. For example, the addition of ionic species such as ION E increased the crack-onset strain up to 115%; this result was attributed to enlarged PSS^- domains resulting from morphological changes.[54] Another strategy involves incorporating additives into the PEDOT:PSS matrix. High-molecular-weight PSSNa increases the PSS^- content, and raises the crack-onset strain to 70%.[54]

To further improve hole injection capabilities, tuning the WF of the HIL is crucial for optimizing device efficiency. When perfluorosulfonic acid (PFSA), which contains fluorine-rich functional groups, is blended with PEDOT:PSS, the PFSA self-assembles at the top surface of the HIL; this distribution causes formation of a fluorine concentration gradient that decreases from top to bottom (Figure 5F).[55–59] The high ionization energy of fluorine causes the WF to increase gradually with fluorine concentration, and can reach WF up to 5.9 eV.[55] This elevated WF greatly facilitates hole injection into the stretchable light-emitting layer, and thereby significantly increases device efficiency.[56]

Incorporating an HTL in ISOLEDs can further improve hole injection, transport, and electron blocking. When selecting HTL, factors such as morphological and thermal stability are as crucial as hole mobility and WF.[60] HTLs, such as triarylamines and benzidine-based materials commonly used in conventional OLEDs, should be amorphous, possess high thermal stability, and exhibit a glass transition temperature $T_g > 100$ °C.[60] However, small-molecule transport materials often crystallize due to their low T_g and low crystallization temperature T_c; this phenomenon can lead to device degradation under thermal stress. The HTL must be thermally stable to minimize morphological changes and prevent crystallization caused by heat from non-radiative recombination or Joule heating during operation (**Figure 6A**).

The T_g of HTLs poses a limitation for their use in ISOLEDs due to low mechanical deformability. Even polymeric HTLs like *N,N′*-Bis(3-methylphenyl)-*N,N′*-diphenylbenzidine (poly-TPD), poly[bis(4-phenyl)(2,4,6-trimethylphenyl)amine] (PTAA), poly(9-vinylcarbazole)

(PVK), and poly[(9,9-dioctylfluorenyl-2,7-diyl)-co-(4,4′-(*N*-(4-sec-butylphenyl) diphenylamine)] (TFB) are inherently brittle because of their $T_g > 100$ °C. To adapt these materials for ISOLEDs, a systematic approach is needed to incorporate stretchability. An effective strategy is to blend these HTLs with elastomeric materials, combining the stretchability of soft polymer chains with the hole injection and transport capabilities of the HTLs. This composite structure can be tuned to achieve the balance between mechanical flexibility and transport properties that is essential for durable, highly-efficient ISOLEDs.

Elastomers like polyurethane and SEBS-*g*-MA have been used effectively as matrices for stretchable HTLs in ISOLEDs (Figure 6B). HTL stretchability has been increased either by achieving a homogeneous blend with elastomers or by promoting controlled phase separation within the blend. TFB, a polymeric HTL with high hole mobility $\mu_h \approx 10^{-3}$ cm^2 V^{-1} s^{-1},[61] has excellent miscibility with polyurethane, with which it forms a uniform blend. This TFB:PU blend can withstand strains up to 100% without cracking, while a rigid TFB film without polyurethane exhibits a crack-onset strain of less than 25%.[62] Additionally, the TFB:PU blend increases the work function to 5.5 eV, which further reduces the hole injection barrier that can persist even when PEDOT:PSS is used as the HIL.

In contrast, TFB has limited miscibility with polystyrene-block-poly(ethylene-ran-butylene)-block-polystyrene-graft-maleic anhydride (SEBS-g-MA), so the blend undergoes phase separation, and TFB islands form at the base of the composite film; they increase the stretchability of the film, and achieve a crack-onset strain >50%.[18]

Additionally, CdSe:ZnS quantum dots (QDs), which are commonly used as emitters, blend well with elastomeric matrices, so an emissive layer fabricated from a QD:SEBS-g-MA:TFB solution forms a uniform QD:SEBS-g-MA layer on top of localized TFB islands. This vertically stratified structure, featuring a TFB-rich layer at the base to serve as hole transport pathways, enables effective hole injection and transport into the emissive layer.

Despite these advances in developing stretchable HTLs by material engineering, challenges remain. The inherent rigidity of HTL limits their potential in ISOLED applications. Elastomers are insulators; thus, while their incorporation improves stretchability, it often reduces the efficiency of both electron injection and electron transport. Thus, new approaches must be found to develop intrinsically stretchable transport materials or to modulate their excitonic properties, to optimize the balance between stretchability and charge transport capabilities.

5. Intrinsically Stretchable Light-Emitting Materials

The molecular structure of the material determines its properties. Long-range ordered structures improve electrical properties but also increase rigidity, and thus decrease stretchability compared to short-range ordered structures. Therefore, a crucial task in developing ISOLEDs is to optimize both the mechanical and electrical functionalities of stretchable light-emitting materials.

The stretchability of conducting films is commonly compared using the normalized resistance change (resistance while stretched divided by resistance while relaxed). under static or cyclic tensile strain. However, a well-established definition for the stretchability of light-emitting materials is lacking. From a mechanical characterization perspective, the stretchability of these materials may be determined by the fracture strain or crack-onset strain using film-on-water or film-on-elastomer tensile stretching tests.[63] Formation and propagation of cracks degrade the electrical properties of the thin film; therefore, increasing the crack-onset strain is essential to maintain structural integrity under stretching.

The stretchable light-emitting material is commonly deposited on stretchable TCE, then sandwiched by another electrode; the presence of that top electrode can delocalize the strain and may thereby lead to crack formation.[64] Therefore, the film-on-elastomer tensile stretching test is closer to the practical situation than the film-on-water test. The stretchability of the light-emitting material can be characterized by its crack-onset strain, with high values indicating good stretchability. The light-emitting materials show a trade-off relationship between stretchability and electrical properties, similar to stretchable TCEs.

The conjugated light-emitting polymer Super Yellow (SY) possesses a rigid phenylenevinylene backbone and is therefore not stretchable. One approach to achieve stretchable light-emitting

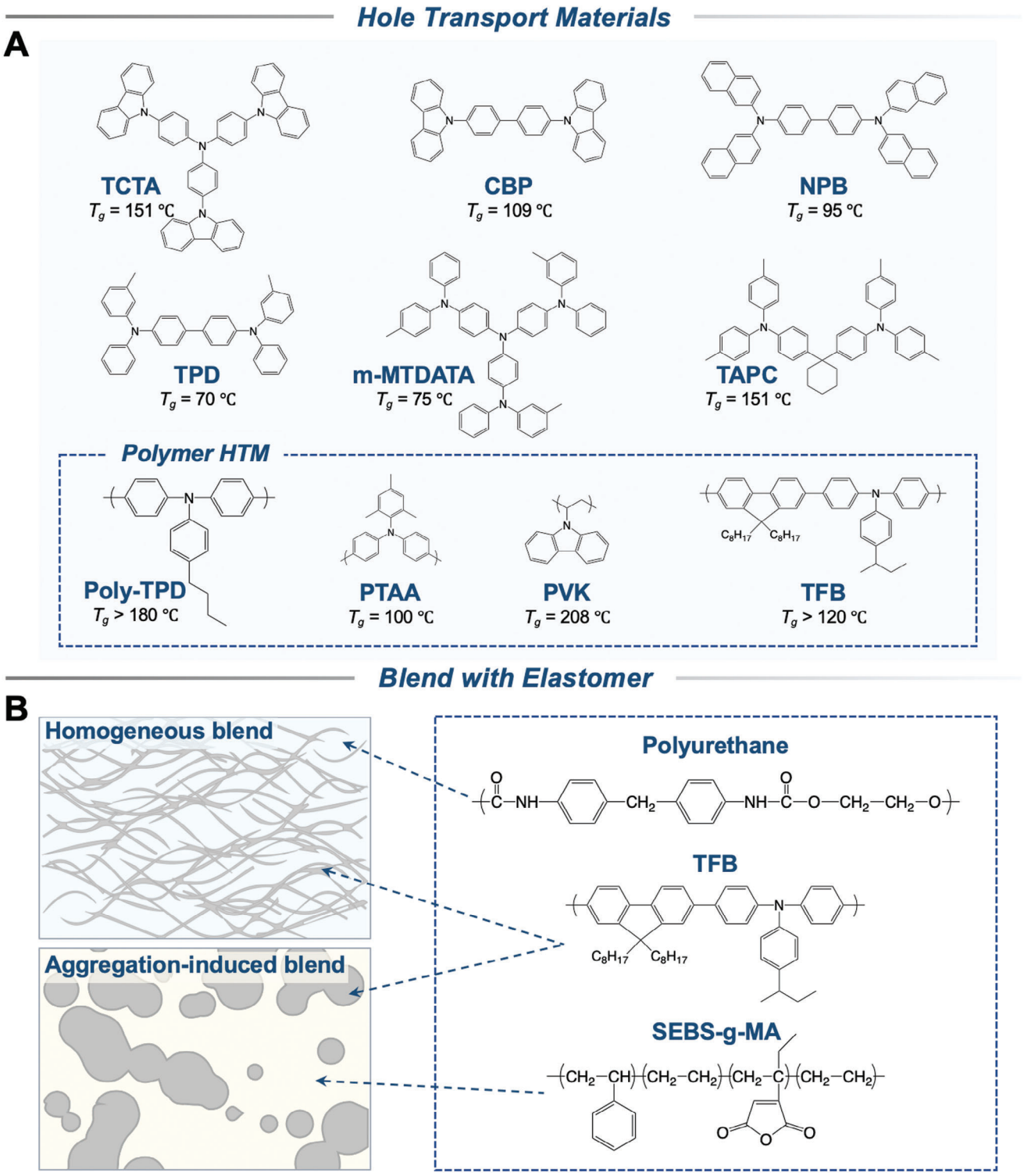

Figure 6. A) Chemical structures of representative solution-processable hole transport materials. B) Morphologies of TFB blended with different elastomers.

materials is to use a multicomponent system in which additives are used to plasticize the light-emitting polymer. If these additives have low T_g, they lower the T_g of the composite as a result of the rule of mixture. This blending process has the potential to reduce intermolecular interactions and increase chain mobility, and thereby increase the mechanical flexibility and stretchability.

Poly (ethylene oxide) (PEO) with a $T_g \approx -50$ °C has great chain flexibility and can also serve as ionic conductive medium for electrochemical light-emitting cells, in which dissociated ions under electric field can induce severe band bending that facilitates charge injections at the interface.[65] The composite was modified by incorporating a crosslinker, ethoxylated trimethylpropanetriacrylate (ETPTA), and lithium trifluoro-methanesulfonate (LiTf); the result is a soft electrolyte composed of PEO, ETPTA, and LiTf, which forms island phases with an average diameter≈100 nm (**Figure 7A**). The formation of these island phases is facilitated by the stronger polarity of the electrolyte compared to SY. The electrolyte has $Y = 72$ MPa, primarily attributed to the viscoelastic properties of PEO, whereas SY has $Y = 178$ MPa. Overall, Y of the composite has been significantly reduced to 100 MPa.[66] ETPTA contains moieties that are compatible with both PEO and SY, so the crosslinked ETPTA network has an important function in increasing the mechanical integrity at the interface between the ionic phase and SY networks.[67] In pristine SY, the polymer chains reorient and align in the stretching direction, so light emission becomes anisotropic, and is particularly weak perpendicular to the stretching direction. However, in the composite, the soft ionic phase adapts to the deformation, and thereby ensures the continuity of the SY phase and promotes isotropic light-emitting properties.

Incorporation of polymers into nanofibril structures by exploiting conjugated-polymer/elastomer phase separation-induced elasticity is another promising approach to achieve stretchable applications.[68] This "nanoconfinement" effect can lower both T_g, and Y of the composite, and thereby achieve a significant improvement in stretchability. When SY polymer is blended with a polyurethane elastomer matrix, nanofibril structures become uniformly distributed throughout the material, without any concentration gradient in the thickness direction (Figure 7B).[62] The polarity of the carboxylate group in the polyurethane ensures the miscibility between SY and polyurethane, and thus prevents strong phase separation and formation of undesired morphologies. This blending process leads to a decrease in the π–π stacking distance and an increase in the coherence length; these changes improve the charge-transport properties without compromising the stretchability of the material.

Similarly, by incorporating a non-ionic surfactant Triton X, which possesses large hydrophobic head and hydrophilic tail groups, a similar morphology with nanofibril structures can be achieved (Figure 7C).[53] The addition of Triton X evokes a conformational transition of the polymer from coiled to linear. This transition decreases interchain interactions and increases the free volume within the material. Consequently, T_g of the film is lowered from 82.1 to 51.6 °C, and the onset strain for crack formation is increased from 40% to 110%. Use of nanoconfinement increases stretchability of the light-emitting materials without causing significant degradation in their electrical properties.

Formation of nanofibrils with an extended coherence length can increase intrachain charge transport, but it can also decrease interchain charge transport at the junctions between nanofibrils. Achieving a balance between these two competing transport mechanisms presents a significant challenge when incorporating non-conjugated soft materials into light-emitting blends. Furthermore, to obtain the desired nanofibril structure, the phase separation between the light-emitting material and the non-conjugated soft materials must be precisely controlled. However, this requirement for precise control of phase separation may limit the applicability of this approach to subsets of light-emitting materials and elastomers.

The primary objective is to synthesize a single-component stretchable electroluminescent material that allows for precise control over its optical, electrical, and mechanical properties. This objective can be accomplished by exploiting the anionic polymerization of pyrene, styrene, and butadiene to achieve a triblock copolymer structure (Figure 7D).[69] Within the film, the pyrene segments undergo strong π-π interactions, which cause the formation of rigid domains. These domains retain their charge-injection capabilities even under stretching conditions. During polymerization, pyrene has a lower concentration than styrene and butadiene, so the rigid domains are surrounded by flexible polybutadiene domains. This arrangement yields island-like structures, which allow dissipation of strain energy through the polybutadiene chains during stretching. Although the fracture strain of the stretchable light-emitting material can be increased to 800% after co-polymerization, achieving highly-efficient ISOLEDs requires fine-tuning of the charge transport between the rigid light-emitting domains.

Fluorescent light-emission that relies on singlet excitons has a maximum theoretical quantum yield of 25%, because it is constrained by spin statics. To further boost the efficiency of the ISOLED, thermally-activated delayed fluorescence (TADF) that utilizes both singlet and triplet excitons was developed (Figure 7E).[70] The TADF unit contains acridine as the electron donor and benzophenenone as the acceptor and has a large dihedral angle for efficient TADF process with small energy-level splitting between singlet and triplet excited states. By varying the alkyl chain length in the polymeric backbone on which TADF units are pendant as side groups, the maximum stretchability has been increased to >125%. This increase is attributed to the robust structure of the TADF units and the flexibility conferred by the long alkyl backbone. Under applied strain, charge carrier hopping transport and light-emitting properties are minimally affected; this result demonstrates the stability and efficiency of the system that exploits TADF.

The development of intrinsically stretchable light-emitting materials has been significantly advanced by blending light-emitting materials with elastomers and using long flexible alkyl chains to modify the backbones of light-emitting materials. Despite the notable increase in the stretchability of the light-emitting layer, the devices that use stretchable materials, even on rigid substrates, still have inferior light-emitting efficiency of compared to OLEDs prepared using physical vapor deposition (**Table 2**).

To increase understanding of the charge-carrier dynamics in the stretchable light-emitting layer, particularly during stretching, further analysis is necessary. This analysis can provide valuable insights for material design and optimization. Additionally, crosslinking the light-emitting layer presents an alternative

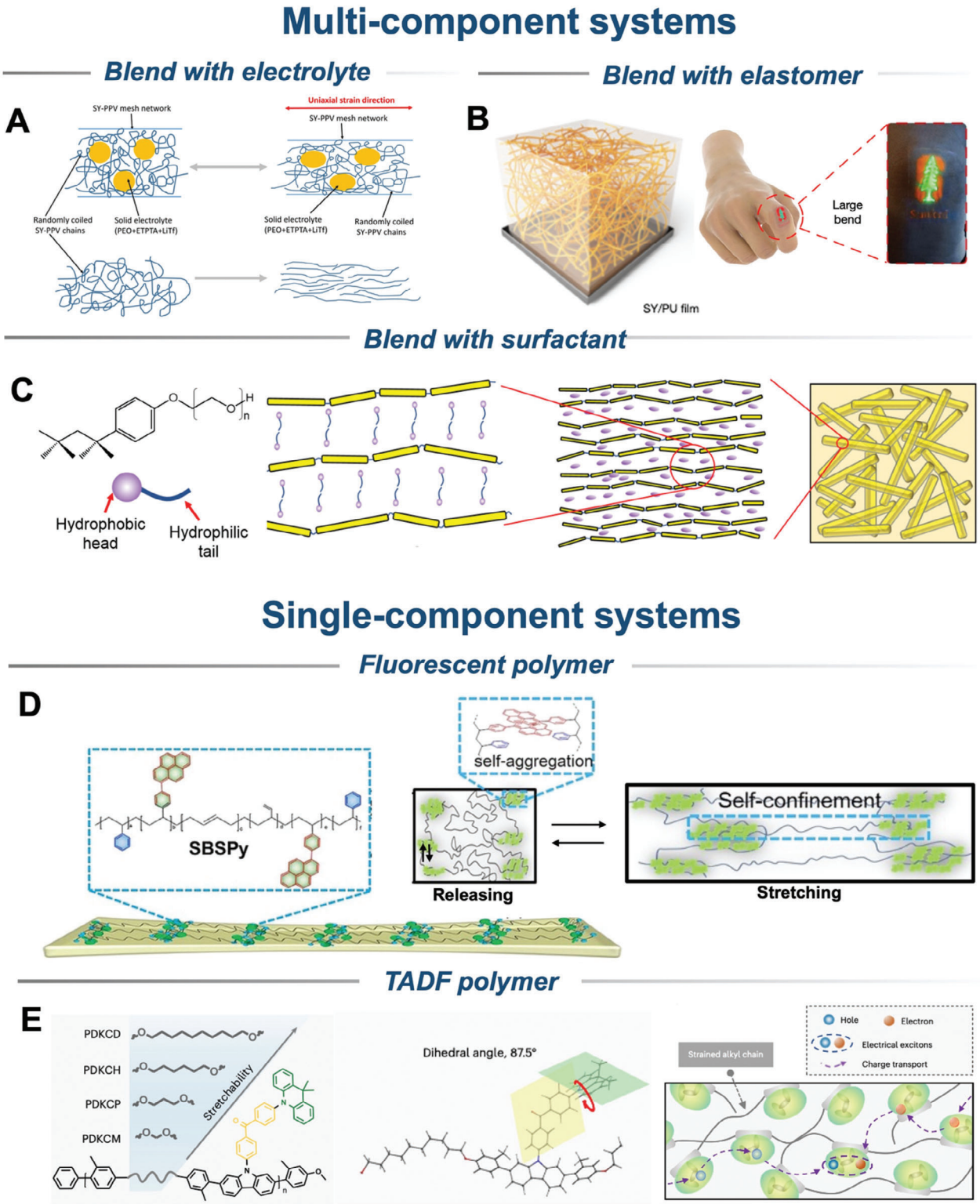

Figure 7. Strategies to achieve intrinsically stretchable light-emitting materials for display applications. A) Blending commercialized light-emitting polymer super yellow (SY) with viscoelastic polymer polyethylene oxide (PEO) and solid electrolyte as the stretchable light-emitting layer. Reproduced with permission.[66] Copyright 2016, American Chemical Society. Blending SY with B) elastomer or C) non-ionic surfactant to lower the glass transition temperature and attain the nanofibril structure. Reproduced with permission.[62] Copyright 2022, Springer Nature. Reproduced with permission.[53] Copyright 2021, American Association for the Advancement of Science. D) Co-polymerization of the light-emitting unit with elastomer. Reproduced with permission.[69] Copyright 2022, WILEY-VCH. E) Insertion of long alkyl spacer in the polymer backbone of TADF light-emitting polymer. Reproduced with permission.[70] Copyright 2023, Springer Nature.

Table 2. Comparison of State-of-the-Art ISOLEDs and Stretchable Light-Emitting Materials.

Types of stretchable light-emitting materials		Anode	Cathode	L_{max} [cd m^{-2}]	CE [cd A^{-1}]	EQE [%]	V_{on} [V]	Stretchability [%]
Single Component	PDKCD[70]	AgNW/TPU/PDMS	AgNW/TPU/PDMS	2175	10.2	3.3	4.75	60
	SBSPy-16[69]	PEODT:PSS	LiF/Al	3274	5.23	2.08	9.3	54
	PF-MC8[92]	ITO	LiF/Al	1976	–	1.06	5.5	55
Multi Component	SY:Triton X[24]	AgNW/Graphene/SEBS	AgNW/Graphene/SEBS	2185	20.3	–	5.3	73
	SY:PEO:ETPTA:LiTf[36]	AgNW/PUA	AgNW/PUA	2200	11.4	–	6.8	120
	SY:PU[62]	PEDTOT:PSS/PR	PEDTOT:PSS/PR	7450	10.5	–	5	100
	White light-emitting polymer/OXD-7[37]	GO-AgNW/PUA	GO-AgNW/PUA	1100	4	–	7	130
	SY:PEO:KCF_3SO_3[35]	AgNW/Graphene/SEBS	AgNW/Graphene/SEBS	1754	3.14	–	3.7	70
	L-SY-PPV/PAN[93]	Au/AgNW/PDMS	Ag/AgNW/PDMS	3780	2.35	2.64	6.5	30
	SY:Triton X[53]	AgNW/PDMS	AgNW/PDMS	4400	1.6	–	8	80
	PF-B/PEO-DMA/LiTf[67]	SWNT/PtBA	SWNT/PtBA	200	1.24	–	4.5	45
	PFO:SEBS[94]	ITO	Al	2167	–	–	<5	100
	PVK:$Ir(ppy)_3$:L64[95]	ITO	Al	5400	25.3	6.89	–	100
	QD:SEBS-g-MA:TFB[18]	AgNW:PEDOT:PSS	AgNW/Ag/EGaIn	15 170	5.0	1.2	3.2	50

technique to enhance both the stretchability and reliability of ISOLEDs. By controlling the degree of crosslinking, a stretchable light-emitting layer with a tunable *Y* can be achieved. Matching the *Y* of the light-emitting layer with the *Y* of the adjacent charge transport or charge injection layer can mitigate delamination problems caused by Poisson's contraction during stretching. Moreover, side chain engineering can be explored to tune the elasticity of the emitting materials. Incorporating long alkyl side chains can increase the proportion of soft domains and may increase the stretchability.

6. Intrinsically Stretchable Electron Injection/Transport Materials

The low EA of organic light-emitting materials often results in a substantial electron-injection barrier at the cathode/EML interface, and directly reduces both efficiency and operational lifetime in OLEDs. Overcoming this barrier is essential to achieving efficient charge carrier injection, typically addressed by incorporating an ETL with high electron mobility and properly aligned energy levels to form an Ohmic contact (**Figure 8A**). ETLs facilitate electron transport and injection into the EML, and also confine holes within the EML, and thereby help to maintain charge balance within the EML. Optimal ETLs require properties such as high electron mobility, hole-blocking capability, and a low WF, all of which contribute to efficient electron transfer while preventing charge imbalance.[71]

EIL materials further improve electron injection, either by increasing the ETL's conductivity by n-type doping or by forming an interfacial dipole that reduces the injection barrier (Figure 8B). Developing n-type dopants for ETLs presents a challenge, because effective dopants require a highest occupied molecular orbital (HOMO) level higher than the ETL's lowest unoccupied molecular orbital (LUMO), which is typically around −3.0 eV. However, high HOMO levels can lead to instability of the dopant in air, and this trend complicates the development of reliable n-type dopants.[46] An alternative approach involves inducing dipole formation at the cathode interface to shift the vacuum level and reduce the electron injection barrier. This approach supports efficient electron injection without the instability associated with conventional n-type dopants, and thereby improves device efficiency.

Inorganic compounds, amine-derived organic materials, and ionic salts are as promising solution-processable EILs for ISOLEDs. Among inorganic EILs, alkali metal compounds like lithium and cesium are commonly used to adjust the cathode WF (Figure 8C). For example, lithium fluoride (LiF) interacts with metallic cathodes (typically aluminum), and thereby facilitates Li^+ ion diffusion into the ETL and consequently shifts the Fermi level.[72] Cesium compounds, such as cesium carbonate (Cs_2CO_3) operate similarly: cesium's low WF (≈2 eV) provides effective n-doping, and Cs^+ diffuses into the EML only to a limited extent, and therefore does not decrease device stability.[73] However, the brittleness of these crystalline inorganic materials complicates their use in ISOLEDs, which demand mechanical flexibility.

Conjugated polyelectrolytes (CPEs) such as poly(9,9-bis(3′-(N,N-dimethyl)-N-ethylammoinium-propyl-2,7-fluorene)-alt-2,7-(9,9-dioctylfluorene))dibromide (PFN-Br) and crown-conjugated polyelectrolyte (Crown CPE) are effective EIL materials for ISOLEDs. CPEs have alternating fluorene and phenylene backbones with sulfonate-terminated alkyl side chains and counter ions; this structure increases electron injection and electron transport. The conjugated polymer backbone is planar, and therefore forms an efficient charge injection pathway and promotes self-orientation of sulfonate groups and counter ions; this process creates a substantial interfacial dipole.[74] This interfacial dipole effectively lowers the electron-injection barrier, and thereby facilitates electron transport and injection into adjacent layers. However, the planar conjugated structure of CPEs is also a limitation, because it hinders n-doping ability due to the low content of polar moieties at the interface with the EML.

Amine-derived polymers like polyethyleneimine (PEI) and polyethyleneimine ethoxylated (PEIE) have strong n-doping

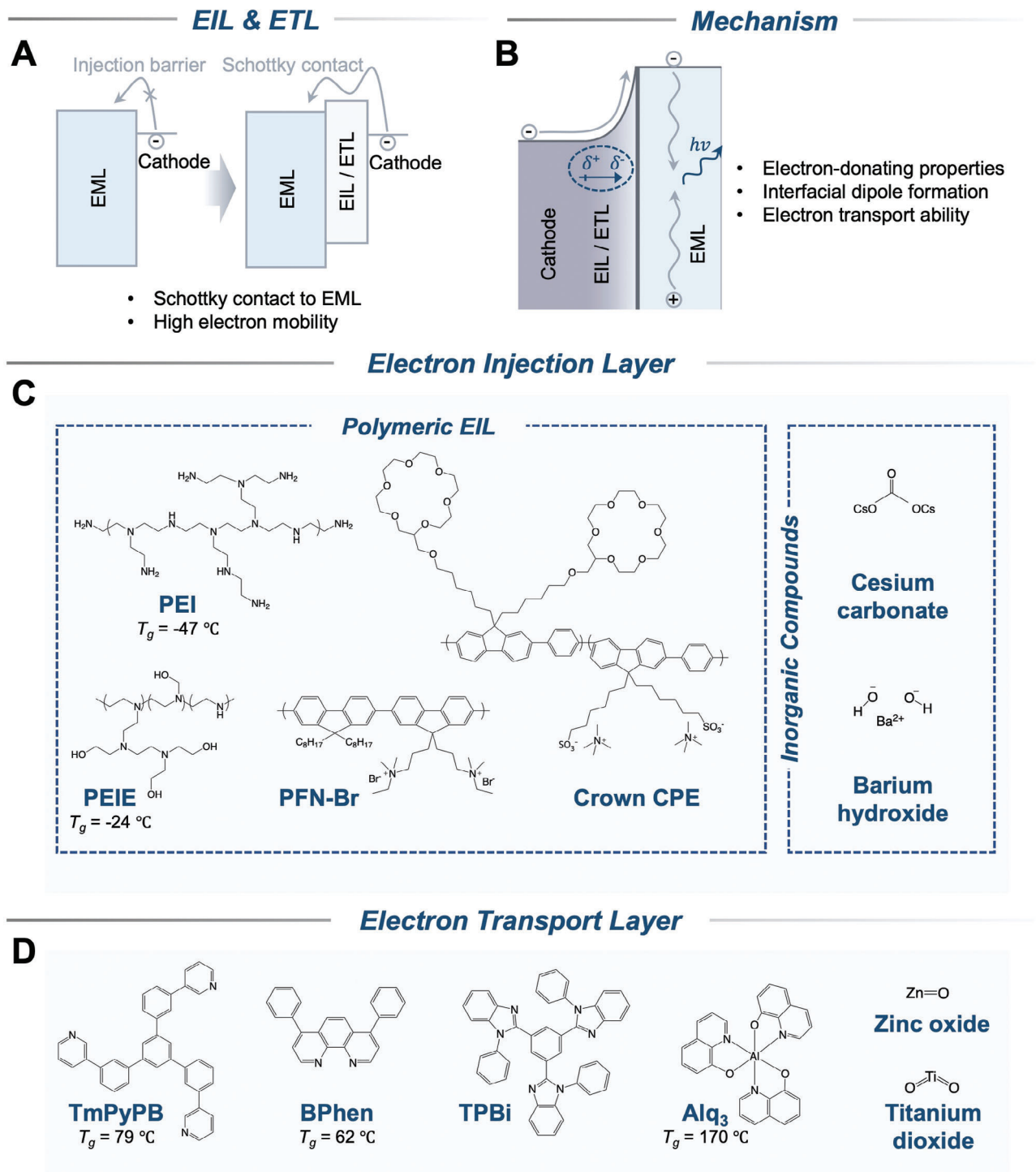

Figure 8. A) Schematic illustration of the energy band diagram with and without electron-injection layer (EIL)/electron transport layer (ETL). B) Mechanism of electron injection at cathode interface. C) Chemical structures of representative solution-processable EILs. D) Chemical structures of representative solution-processable ETLs.

ability and excellent band alignment properties, and are therefore effective EIL materials. The amorphous morphology of PEI and PEIE enables strong n-doping.[74] The protonation of abundant amine groups provides N^+ ions, which form dipoles at the cathode interface by elevating the vacuum level and lowering the electron injection barrier. These amine-rich polymers are non-conjugated insulating materials that lack inherent electron-transport capabilities and are often combined with other EIL or ETL materials that have higher electron mobility than the polymers. For instance, PFN-Br, which has an electron mobility of

8.47×10^{-4} cm^2 V^{-1} s^{-1}, shows synergistic effects when blended with PEIE.[75] The WF of a ZnO layer decreases from 4.21 to 3.65 eV after deposition of PEIE, and to 3.64 eV after deposition of PFN-Br.[76] A blend of PEIE and PFN-Br further reduces the cathode's WF to 3.46 eV, likely due to strengthened fluorene-fluorene interactions in PFN-Br. This PEIE:PFN-Br blend also has excellent stretchability, with no visible cracks even at 100% strain.[62]

Deposition of crown-CPE on a PEI layer also effectively reduces the cathode's WF while maintaining stretchability, with a crack-onset strain >70%.[24] Applying PEI as a WF-modifying layer reduces the WF of the stretchable cathode from 4.60 to 4.04 eV. When crown-CPE is deposited on PEI, the crown-CPE undergoes self-orientation with tetramethylammonium ions and sulfonate ions aligned at the surface. The crown ethers in the CPE's side chains tend to hydrogen bond with the amine groups in PEI, and thus further reduce the WF to 3.57 eV.

Amine-derived polymers can also serve as stretchable matrices in composite layers with rigid interfacial materials. Most conventional electron transport materials lack mechanical flexibility (Figure 8D), and therefore have limited applicability in ISOLEDs. A composite cathode interfacial layer that integrates transport materials (e.g., ZnO) with stretchable injection materials can achieve both mechanical deformability and effective electron injection. The stretchability of the PEIE:ZnO composite alone is limited, with microcracks forming at 20% strain; however, an EML deposited on this layer retains a smooth, crack-free surface up to 60% strain, and maintains stable device initial luminance up to 50% strain.[18]

In cases where the cathode WF can be reduced to≈2 eV, efficient electron injection might negate the need for an additional ETL. Such an ultra-low work function can be achieved using superbases, like 2,6-bis(1,3,4,6,7,8-tetrahydro-2H-pyrimido[1,2-a]pyrimidin-1-yl)pyridine, that facilitates direct electron injection into the EML through coordination and hydrogen bonding.

However, due to limitations in material characteristics, currently available stretchable cathodes typically have a WF > 2.9 eV. Developing materials that enable ultra low WF, perhaps by incorporating compounds like superbases, could yield simplified ISOLED structures and increased electron injection efficiency.[77]

7. Wearable/Flexible Systems Integrated with Light-Emitting Diodes

The rise of wearable electronics has accelerated the development of flexible and wearable displays, like smart watches and glasses. As displays become the primary mode of human-machine interaction, the integration of displays directly onto the human skin has become highly desirable for seamless communication. To achieve this goal, displays must be stretchable in all directions, and must establish conformal contact with the skin. However, current stretchable displays, especially intrinsically stretchable ones, may not yet meet industrial standards concerning maximum luminance, operating voltage, external quantum efficiency, and operational stability. Nonetheless, wearable and flexible electronic systems equipped with light-emitting diodes offer valuable insights for the future application of ISOLEDs. Despite the deficiencies of ISOLEDs, these integrated systems that use them illustrate their various practical applications. Continued research and development are necessary to overcome the current limitations and fully unlock the capabilities of ISOLEDs for stretchable display technology and beyond. To utilize ISOLEDs as a wearable platform for information output, they must be developed into matrix arrays. These arrays can be categorized into passive-matrix (PM) and active-matrix (AM) types, depending on the driving circuits employed.

In PM arrays, light-emitting units are defined in the region where cathode and anode lines overlap, and the light emission is controlled by applying voltage line by line. Recent advances include PM ISOLED arrays that use graphene-derived transparent conductive electrodes on a 3-inch five-by-five PM configuration (**Figure 9A**).[24] These arrays withstood a maximum linear strain of 20.3% that was applied using the convex stretching method, with an axis moving upward to apply tensile strain. However, a challenge arises when aiming for high-resolution displays with micrometer-scale sized pixels . Such displays can result in a notable voltage drop within the electrodes, and this phenomenon may lead to increased operation voltage for PM ISOLED arrays in the future. To achieve high-resolution wearable displays that consume energy efficiently, this limitation must be overcome.

As an alternative, AM arrays are essential for high-resolution display applications. Each pixel is connected with thin film transistors (TFTs) that can turn it on and off individually; this arrangement in an ISOLED display increases its resolution, reduces its lower power consumption, increases its response speed, and enables precise control of each pixel. However, monolithically integrating the ISOLED into TFTs remains a significant challenge in both the materials and the engineering aspects. Only one work has successfully integrated the ISOLED with the intrinsically stretchable TFTs, and achieved two-by-three arrays that can endure 30% tensile strain.[3] However, due to the complexity of the device integration, the ISOLED efficiency is inferior to that of commercialized OLED displays. Overcoming this challenge and improving ISOLED efficiency in AM arrays are vital steps to advance this technology for practical high-resolution display applications.

Ultrathin, flexible AM arrays deposited on molybdenum disulfide (MoS_2) TFT backplanes, with a total thickness of ≈7 µm, have been developed (Figure 9B).[78] These flexible OLED displays can conformally contact human skin, and thereby demonstrate the feasibility of wearable displays directly applied to human skin. Once AM displays are achieved, the next critical steps are to integrate various functionalities such as sensing, processing, and signal transmission units in wearable systems. This integration enables seamless user interaction by emphasizing the value of real-time signal visualization in a human-readable and convenient manner without the need for additional data storage or processing units. Replacing the rigid or flexible LEDs typically used in wearable monitoring devices with ISOLEDs offers significant advantages, because their intrinsic stretchability makes them ideal for skin-attached wearable devices.

LEDs play essential roles in wearable monitoring systems, serving primarily in three applications: as information visualization displays, as light sources for optical sensors, or as integrated devices combining both visualization and sensing capabilities. For instance, when used exclusively for information visualization, LEDs can be integrated into systems for temperature sensing, motion detection, and electrocardiogram (ECG)

Matrix arrays

Passive matrix

A

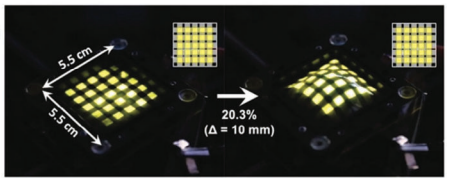

Active matrix

B

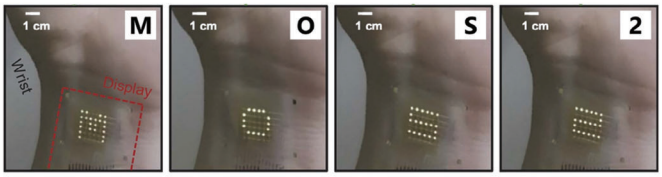

Display applications

Singal visualization

Temperature & Step sensor

C

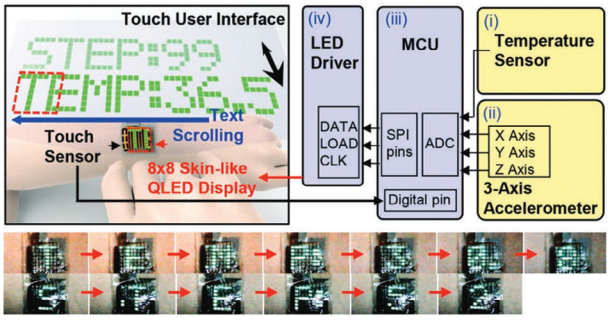

ECG monitor

D

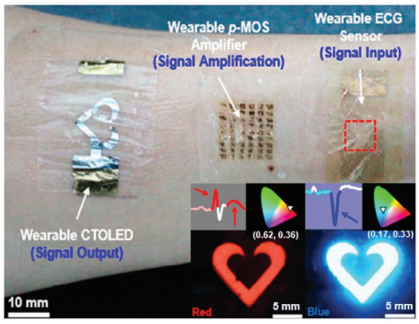

Sensor applications

PPG sensor

E

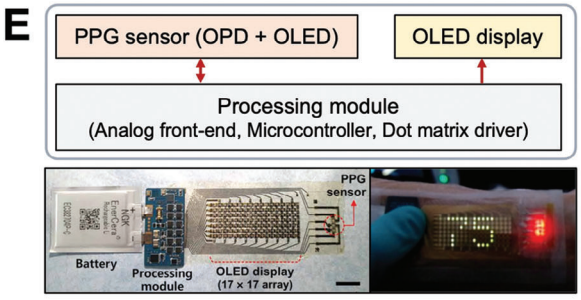

Pulse oximeter

F

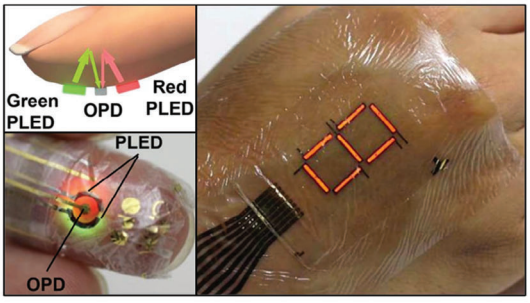

Simultaneous Sensing & Visualize

Pressure visualization

G

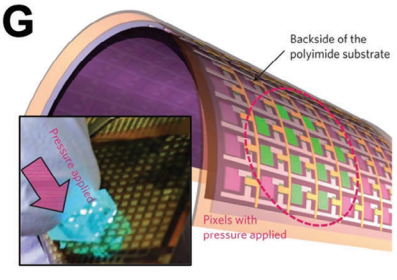

Light interaction

H

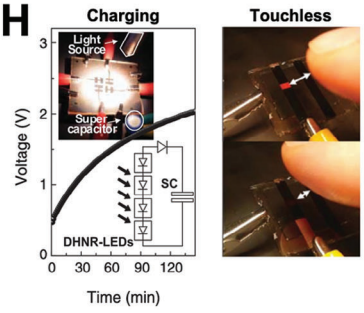

Integrated system

User interaction

I

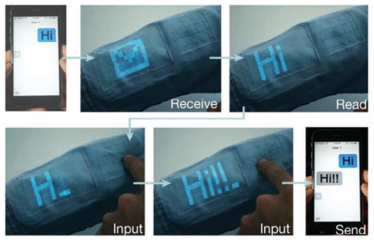

monitoring. In these applications, the LED-based systems enable comprehensive monitoring of external signals, such as temperature and movement, and of internal biosignals transmitted from various sensors. Incorporating ISOLEDs into these systems can enhance their flexibility, durability, and compatibility with dynamic, on-skin environments.

Temperature sensing to prevent skin burns and step counting for activity tracking are critical functionalities in on-skin wearable devices, enabling them to effectively monitor external dangers and user activities, and thereby ensuring user safety and health (Figure 9C).[79] These capabilities are achieved by integrating a temperature sensor and an accelerometer with ISOLEDs, to enable real-time collection and visualization of data.

The common temperature sensor functions by detecting variations in the forward voltage drop across a semiconductor diode.[80] As temperature rises, the thermal energy of electrons increases; this change reduces the barrier potential and causes a corresponding decrease in the forward-voltage drop. This well-characterized relationship between temperature and voltage drop allows for precise temperature measurements. These sensors are essential for avoiding potential skin burns caused by prolonged heat exposure or for monitoring elevated body temperature during physical activities.

The accelerometer measures the magnitude and direction of acceleration vectors resulting from user movement. This sensor utilizes microelectromechanical systems technology, which involves a small mass suspended within a microscopic framework by springs. During motion, the mass displaces relative to its frame, and thereby alters either the device's capacitance or resistance. These changes are then converted to electrical signals proportional to the applied acceleration. By continuously tracking changes across multiple axes, the accelerometer accurately monitors motion patterns, and thereby enables functions such as step counting and activity tracking.

By integrating these sensors with ISOLEDs, both environmental temperature, and user movement can be continuously monitored and displayed in real time. This integration provides real-time feedback for activity tracking and safety monitoring, thereby increasing the overall functionality and user experience of wearable devices in a variety of applications.

ECG signals provide vital information about cardiac conditions such as arrhythmias and myocardial infarction (Figure 9D).[81] During each heartbeat, action potentials are generated and spread throughout the body; these electrical impulses are detected by skin-attached ultrathin electrodes, providing essential data for analyzing heart health. A normal ECG waveform consists of PQRST waves, each of which represents a specific aspect of cardiac activity. The P wave represents atrial depolarization, and thus signals the electrical activation that triggers atrial contraction. The Q wave is the initial negative deflection, the R wave is the first positive deflection, and the S wave is the subsequent negative deflection, collectively indicating ventricular depolarization. The T wave corresponds to ventricular repolarization, which mark the recovery phase as the heart prepares for the next beat. Key intervals derived from these waves, such as the PR interval measuring electrical conduction from the atria to the ventricles, the QT interval representing total ventricular electrical activity, and the ST segment indicating ventricular depolarization, are critical for diagnosing various cardiac conditions. By analyzing the shape, size, and timing of the PQRST waves, clinicians can diagnose various heart conditions, such as arrhythmias, myocardial infarction, and conduction disorders.

After being detected by the sensors, the signals are filtered to remove noise, and processed by the system's microcontroller. The microcontroller converts these signals to digital formats that are compatible with the display array, and thus enable real-time visualization. Replacing rigid LEDs with ISOLED displays can increase user comfort by allowing the device to conform to skin deformation during movement, and increase device functionality by ensuring continuous visualization of information. Their stretchability provides a significant advantage, particularly for high-activity applications, in which mechanical reliability and seamless operation are crucial.

LEDs are no longer limited to standalone visualization display; they can perform dual functions as both light sources for sensors and visualization displays, particularly in systems like photoplethysmography (PPG) sensors and pulse oximeters. PPG sensors monitor heart rate by detecting blood flow, using LEDs as emitters and organic photodiodes (OPDs) as receivers (Figure 9E).[12] In these systems, the sensor LED emits red light, which interacts with blood by being absorbed, transmitted, or reflected.

During heart contractions (systole), the increased blood volume leads to greater absorption of red light, reducing the amount reflected back to the OPD, which is indicative of increased cardiac activity. Conversely, during relaxation (diastole), the decreased blood volume allows a higher proportion of red light to be

Figure 9. Applications of flexible/stretchable displays for wearable applications. A) Image of three-inch five-by-five passive-matrix ISOLED arrays that are deformed using convex stretching method. Reproduced with permission.[24] Copyright 2022, WILEY-VCH. B) Active-matrix OLED display arrays using MoS_2 as the TFT back plane showing letters "M", "O", "S", and "2" on a human wrist. Reproduced with permission.[78] Copyright 2018, American Association for the Advancement of Science. C) (top) Schematic illustration of displaying data with signal processing flow, (bottom) photographs of wearable QLED display visualizing the temperature and step counts. Reproduced with permission.[79] Copyright 2017, WILEY-VCH. D) Photograph of the wearable ECG monitoring system on skin. The inset shows color change emission of wearable OLED depending on (left) normal and (right) abnormal ECG signal shape with CIE coordinates of each emission. Reproduced with permission.[81] Copyright 2017, American Chemical Society. E). Photographs of stretchable red OLED arrays with PPG sensors for monitoring cardio signals. Reproduced with permission.[12] Copyright 2021, American Association for the Advancement of Science. F) (top) Principle of pulse oximeter with PLED and OPD, (bottom) photograph of wearable pulse oximeter under operation, and (right) information visualization by 7-segment polymer LED display. Reproduced with permission.[82] Copyright 2016, American Association for the Advancement of Science. G) Vertically integrated TFT, OLED, and pressure sensor arrays for pressure visualization. Reproduced with permission.[83] Copyright 2013, Springer Nature. H) Time-dependent voltage curves of supercapacitors charge by four LEDs (left), and demonstration of touchless interactive display (right). Reproduced with permission.[84] Copyright 2017, American Association for the Advancement of Science. I) Components of the integrated textile system. Photographs of information input from user using integrated textile keyboard. Reproduced with permission.[85] Copyright 2021, Springer Nature.

reflected, indicating reduced cardiac activity. This variation in light intensity enables measurement of heart rate. The PPG waveform offers critical insights into cardiovascular health by representing systolic and diastolic amplitudes, as well as the interval between beats. The systolic amplitude corresponds to the heart's contraction phase, when increased pressure increases blood flow, whereas the dicrotic minimum provides information about arterial elasticity, wave reflections, and overall vascular health. Together, these parameters provide a detailed assessment of blood flow, heart rate, and blood pressure.

Integrating LEDs to enable both sensing and visualizing of PPG signals simplifies the design of wearable health-monitoring devices. Replacing rigid LEDs with ISOLEDs in such systems increases comfort and functionality, because ISOLEDs can conform to skin as it deforms, and thereby minimizes the noise signal that is caused by the air gap between light source and skin.

Similar to PPG sensors, pulse oximeters measure blood oxygenation by detecting light emitted by LEDs and absorbed by hemoglobin within blood erythrocytes, using an organic photodiode (OPD) as the receiver (Figure 9F).[82] In this system, separate LEDs are required for sensing and for visualizing blood oxygenation. Deoxygenated hemoglobin (Hb) binds absorb light differently at specific wavelengths than oxygenated hemoglobin (HbO_2); using red and green LEDs in conjunction with an OPD this difference enables calculation of blood oxygenation levels (SpO_2) as

$$SpO_2 = 100\% \times C\left(HbO_2\right) / \left[C\left(HbO_2\right) + C\left(Hb\right)\right] \quad (4)$$

where C represents concentration.

The detected PPG and pulse oximetry signals are processed and transmitted to the visualization display through several stages. First, the analog signals detected by the sensors are converted by the analog front-end to digital data with amplified intensity. Next, the microcontroller filters out noise from the transformed data and processes it to calculate metrics such as heart rate and SpO_2 level. Finally, a matrix signal processor connected to a dot matrix driver displays the processed data on the device's LED array.

These sensor devices are effective for wearable health monitoring, but are constrained by the rigid form factor of traditional LEDs and OPD components, which can reduce on-skin comfort and adaptability. By replacing traditional LEDs with ISOLEDs, the system's durability, mechanical stability, and comfort can be significantly increased.

LEDs can also function as both sensors and visualization displays simultaneously, and are therefore suitable for applications such as pressure-sensitive displays and light-interactive displays. Pressure sensing is an essential feature for preventing impacts and pressure sores, and is used in on-skin wearable devices to monitor external forces. Pressure visualization using pressure-sensitive rubber (PSR) integrated with OLEDs enables large-area quantitative mapping of applied pressure (Figure 9G).[83] In this configuration, each OLED anode is connected to the drain of a nanotube TFT for active-matrix operation, and the PSR is laminated onto the cathode of the OLEDs. The PSR surface is coated with silver ink, which forms a ground contact. As pressure is applied, conductive carbon nanoparticles embedded within the PSR create tunneling pathways, which reduce the resistance of the PSR. This resistance decrease increases the current flow through the OLEDs, so their brightness increases. Additionally, as the contact area between the PSR and the OLED cathodes grows as pressure increases, the number of activated OLEDs increases. Consequently, the applied pressure's strength is visualized as brightness, while the area of the applied pressure is spatially mapped by the distribution of operating OLEDs. This integration of OLEDs with PSR for pressure visualization demonstrates the potential of ISOLEDs to increase the functionality and reliability of pressure-sensitive displays. Their ability to conform during mechanical stress without compromising device efficiency confirms their suitability for advanced on-skin wearable applications.

Light-responsive on-skin wearable devices are powered by absorbed light energy, so they can detect and display signals from both internal and external sources, and can offer touchless interactions. Double-heterojunction nanorod (DHNR) light-responsive LEDs have a unique energy-band structure that can combine energy harvesting with touchless interactive display capabilities (Figure 9H).[84] DHNRs integrate Type-I and Type-II heterojunctions, with each type serving a distinct function. The Type I heterojunction (e.g., CdSe/CdS and CdSe/ZnSe) achieves high emission efficiency by confining electrons and holes in the same region. Under forward bias, recombination of electron-hole pairs within the Type I heterojunction produces light by electroluminescence. The Type-II heterojunction (e.g., CdS/ZnSe) is optimized for effective photodetection by spatially separating electrons and holes into different regions, and thereby facilitating efficient charge separation. This dual-functionality enables the DHNR LEDs to switch dynamically between light emission and photodetection, depending on the direction of current flow. Under reverse or zero bias, incident photons generate electron-hole pairs that are separated by the Type-II heterojunction; the process generates a photocurrent that can be exploited to detect light. Under forward bias, the device operates in LED mode, and emits light. This versatility allows DHNR LEDs to adjust brightness dynamically in response to external light conditions, and even to recharge by absorbing light from external sources; this ability significantly increases their energy efficiency. These capabilities make DHNR-based devices promising for next-generation wearable systems that require seamless interaction and self-sustaining operation.

The continuous integration of multiple functionalities into wearable systems enables innovative applications and transformative user interactions. Efforts in monolithic integration and wearable system design are driving the evolution of wearable technology, and thus ensuring seamless integration into daily life. The inclusion of power supply, sensors, processing units, transmission modules, and input interfaces in wearable systems will ultimately enable these devices to replace mobile phones in the future (Figure 9I).[85]

Comparisons of numerous electronic systems integrated with displays (**Table 3**) provide valuable insights into the future potential of ISOLEDs for wearable systems. The synergistic combination of diverse functionalities and systems using ISOLEDs has the potential to revolutionize wearable technology. As light-emitting efficiency and operational stability continue to be advanced, ISOLED-equipped wearable systems are in position to transform industries ranging from healthcare and fitness to communication and entertainment. These developments will

Table 3. Comparison of wearable systems with display.

System	Sensor	Power	Display
Flexible wireless energy-harvesting system[62]	–	Wireless power supply	Intrinsically stretchable OLED
Wireless stretchable sensor and display system[54]	Stretchable strain sensor	Stretchable diode	Stretchable electrochromic display (ECD)
Real-time health monitoring patch[12]	Stretchable PPG sensor	Battery	OLED
Multi-modular E-textile bioenergy microgrid system[96]	Na^+ potentiometric sensor	Triboelectric generators/ microbial biofuel cells	ECD
Wearable triboelectric nanogenerator integrated with displays[97]	–	Triboelectric nanogenerator	LCD, LED
User-interactive electronic skin for instantaneous pressure visualization[83]	Pressure sensor	–	Active-matrix OLED array
Organic light emitting board for dynamic interactive display[98]	Floating electrode for touch detection	–	Alternating current electroluminescence
Wearable electrocardiogram monitor[81]	ECG sensing stretchable electrode	–	Color-tunable OLED
Temperature, touch sensing wearable electronics integrated with QD display[79]	Temperature sensor, touch sensor	–	Quantum dot LED
Reflective pulse oximetry device[99]	Organic photodetectors	–	PLED
Visualization and recognition of UV patterns[100]	Organic Photodetectors	–	QLED
Self-healable electronic skin[11]	Pressure/strain/ECG sensor	–	Stretchable ACEL
Light-emitting device integrated with soft gripper[17]	Light sensor	Wireless power supply	Stretchable ACEL

increase user connectivity, personalize experiences, and ultimately improve users' quality of life.

8. Challenges and Opportunities of ISOLEDs

The development of ISOLEDs is still in its early stages, and various problems must be solved to make significant breakthroughs in this field. Currently, ISOLEDs have inferior light-emitting efficiency, maximum luminance, operation voltage, and stability compared to rigid OLEDs. These demerits are mainly a result of the lack of standardized protocols for designing stretchable materials and light-emitting devices. To advance ISOLED technology, several crucial aspects must be considered (**Figure 10**).

From a material perspective, one of the most critical challenges for ISOLEDs is the development of stretchable barrier films. External factors including oxygen and moisture can severely degrade ISOLEDs, and lead to catastrophic failure. To prevent diffusion of oxygen and moisture into the ISOLED, an encapsulation layer is required, and it must also be stretchable. It must achieve an oxygen transmission rate $< 10^{-3}$ cm^3 m^{-2} d^{-1} and a water vapor transmission rate $< 10^{-3}$ m^{-2} d^{-1}.[44] However, the stretchability and barrier properties of the polymer are in a trade-off relationship, so designing a perfect stretchable material for encapsulation is extremely challenging. Consequently, more efforts are needed in material design and engineering to develop suitable encapsulation materials that provide both effective barrier properties and the required stretchability. Addressing both intrinsic and extrinsic stability factors is crucial to improving the operational reliability and lifetime of ISOLEDs.

Most research on ISOLED development has focused on the stretchable light-emitting layer and electrodes, but the stretchable charge transport layers have an equally significant contribution to device efficiency. Electron transport materials are especially important, because they facilitate electron transport while blocking hole transport; this combination of effects is essential for optimizing device efficiency. Additionally, to ensure device reliability, these materials must be mechanically stable under repeated stretching. Therefore, ISOLED materials must be have high elasticity but and also adhere effectively to adjacent layers to prevent mechanical mismatch, which could otherwise lead to device degradation over time.

From a device perspective, the light-emitting efficiency and stretchability of ISOLEDs must be increased. The highest efficiency achieved so far is 20.3 cd A^{-1} using graphene-derived stretchable electrodes, which is comparable to the efficiency of rigid OLEDs on ITO electrodes. Fine-tuning the energy-level alignment at the interface between stretchable electrode and organic materials can increase charge injection and boost ISOLED efficiency. Various approaches include polymer-backbone engineering and the strategic insertion of long alkyl chains to improve charge transport and mechanical flexibility. Alternatively, side-chain engineering and the formation of nanofibril structures via phase separation mechanisms could be explored as effective strategies to enhance both charge injection and stretchability. These strategies hold promise in increasing ISOLED efficiency to rival that of rigid OLEDs.

Furthermore, internal factors such as charge balance, recombination, and charge accumulation at the interface affect the device's operational lifetime. To maximize these traits, the stretchable materials must be electrically and chemically stable to avoid the formation of by-products during device operation. However, studies in these areas are currently lacking, and further research is needed to understand and optimize these intrinsic stability factors.

From a system perspective, the full potential of ISOLEDs can be realized by integrating them with various functional devices, such as driving circuits, sensors, power supply, signal processing,

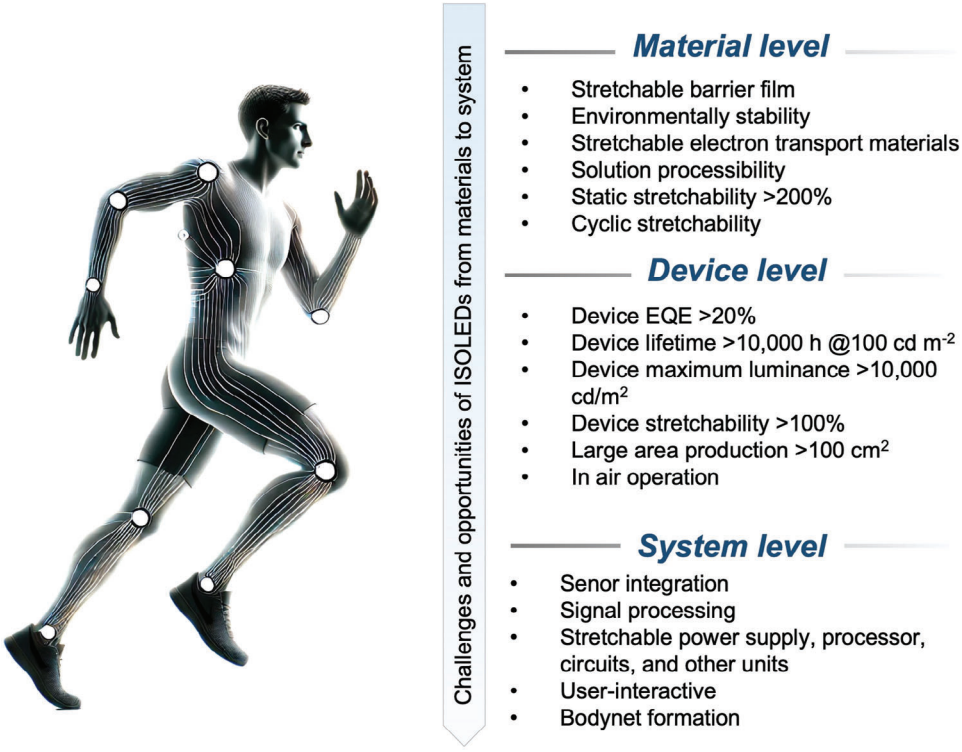

Figure 10. Challenges and opportunities of ISOLEDs across materials, devices, and systems. Key areas include improving material stretchability and charge transport, increasing device efficiency under strain, and exploring system-level integration for advanced applications in wearable electronics.

signal transmission, and input units. This integration will enable a wide range of innovative applications in various industries and daily life scenarios. However, achieving monolithic integration of stretchable devices while maintaining a small size remains a significant challenge. Continued research and development efforts in these areas are vital to overcome the challenges and make significant improvements in ISOLED technology. As progress is made and standards are established, ISOLEDs may have an important contribution to the evolution of flexible and stretchable electronics. They will unlock new possibilities for wearable displays and other stretchable electronic applications, to further enrich our lives and transform how we interact with technology. The combination of functional versatility, stretchability, and adaptability makes ISOLEDs a promising technology with a wide range of potential applications in fields such as healthcare, communication, entertainment, and beyond. As researchers and engineers continue to push the boundaries of ISOLED technology, we can anticipate a future in which flexible and stretchable electronics seamlessly integrate into our lives, and offer increased connectedness and comfort.

Acknowledgements

H.Z., H.-W.K., and W.J.J. contributed equally to this work. This research was supported by the Pioneer Research Center Program through the National Research Foundation of Korea funded by the Ministry of Science, ICT & Future Planning (2022M3C1A3081211). This work was also supported by a National Research Foundation of Korea grant funded by the Korea government Ministry of Science, ICT & Future Planning (2016R1A3B1908431).

Conflict of Interest

The authors declare no conflict of interest.

Keywords

OLEDs, stretchable display, stretchable electrodes, stretchable light-emitting materials

Received: December 19, 2024
Revised: February 4, 2025
Published online:

[1] J. A. Rogers, T. Someya, Y. Huang, *Science.* **2010**, *327*, 1603.
[2] B. Chu, W. Burnett, J. W. Chung, Z. Bao, *Nature.* **2017**, *549*, 328.
[3] T. Sekitani, H. Nakajima, H. Maeda, T. Fukushima, T. Aida, K. Hata, T. Someya, *Nat. Mater.* **2009**, *8*, 494.
[4] H. Zhou, K.-N. Kim, M.-J. Sung, S. J. Han, T.-W Lee, *Device.* **2023**, *1*, 100060.
[5] N. Kim, S. Kee, S. H. Lee, B. H. Lee, Y. H. Kahng, Y.-R. Jo, B.-J. Kim, K. Lee, *Adv. Mater.* **2014**, *26*, 2268.
[6] W. Kwak, J. Yin, S. Wang, J. Chen, *FlexMat.* **2024**, *1*, 5.
[7] M. M. Baig, S. A. Khan, H. Ahmad, J. Liang, G. Zhu, H. Pang, Y. Zhang, *FlexMat.* **2024**, *1*, 79.
[8] L.-Q. Yao, Y. Qin, X.-C. Li, Q. Xue, F. Liu, T. Cheng, G.-J. Li, X. Zhang, W.-Y. Lai, *InfoMat.* **2023**, *5*, e12410.
[9] Y. Wan, X.-C. Li, J. Chen, Q. Wang, C. Liu, C.-F. Liu, W.-Y Lai, *Macromolecules.* **2023**, *56*, 3345.

[10] Y. Wan, X.-C. Li, H. Yuan, D. Liu, W.-Y. Lai, *Adv. Funct. Mater.* **2024**, *34*, 2316550.
[11] D. Son, J. Kang, O. Vardoulis, Y. Kim, N. Matsuhisa, J. Y. Oh, J. W. To, J. Mun, T. Katsumata, Y. Liu, A. F. McGuire, M. Krason, F. Molina-Lopez, J. Ham, U. Kraft, Y. Lee, Y. Yun, J. B. Tok, Z. Bao, *Nat. Nanotechnol.* **2018**, *13*, 1057.
[12] Y. Lee, J. W. Chung, G. H. Lee, H. Kang, J.-Y. Kim, C. Bae, H. Yoo, S. Jeong, H. Cho, S.-G. Kang, J. Y. Jung, D.-W. Lee, S. Gam, S. G. Hahm, Y. Kuzumoto, S. J. Kim, Z. Bao, Y. Hong, Y. Yun, S. Kim, *Sci. Adv.* **2021**, *7*, eabg9180.
[13] L. Yin, M. Cao, K. N. Kim, M. Lin, J.-M. Moon, J. R. Sempionatto, J. Yu, R. Liu, C. Wicker, A. Trifonov, F. Zhang, H. Hu, J. R. Moreto, J. Go, S. Xu, J. Wang, *Nat. Electron.* **2022**, *5*, 694.
[14] H. Zhou, J. Park, Y. Lee, J.-M. Park, J.-H. Kim, J. S. Kim, H.-D. Lee, S. H. Jo, X. Cai, L. Li, X. Sheng, H. J. Yun, J.-W. Park, J.-Y. Sun, T.-W. Lee, *Adv. Mater.* **2020**, *32*, 2001989.
[15] C. Larson, B. Peele, S. Li, S. Robinson, M. Totaro, L. Beccai, B. Mazzolai, R. Shepherd, *Science.* **2016**, *351*, 1071.
[16] H. Zhou, T.-W. Lee, *IEEE Spectrum.* **2020**, *57*, 24.
[17] Y. J. Tan, H. Godaba, G. Chen, S. T. M. Tan, G. Wan, G. Li, P. M. Lee, Y. Cai, S. Li, R. F. Shepherd, J. S. Ho, B. C. K. Tee, *Nat. Mater.* **2020**, *19*, 182.
[18] D. C. Kim, H. Seung, J. Yoo, J. Kim, H. H. Song, J. S. Kim, Y. Kim, K. Y. H. Lee, C. Choi, D. J. Jung, C. Park, H. Heo, J. W. Yang, T. Hyeon, M. K. Choi, D. H. Kim, *Nat. Electron.* **2024**, *7*, 365.
[19] Y. Lee, H. Cho, H. Yoon, H. Kang, H. Yoo, H. Zhou, S. Jeong, G. H. Lee, G. Kim, G.-T. Go, J. Seo, T.-W. Lee, Y. Hong, Y. Yun, *Adv. Mater. Technol.* **2023**, *8*, 2201067.
[20] K. W. Cho, S.-H. Sunwoo, Y. J. Hong, J. H. Koo, J. H. Kim, S. Baik, T. Hyeon, D.-H. Kim, *Chem. Rev.* **2021**, *122*, 5068.
[21] M. S. White, M. Kaltenbrunner, E. D. Głowacki, K. Gutnichenko, G. Kettlgruber, I. Graz, S. Aazou, C. Ulbricht, D. A. M. Egbe, M. C. Miron, Z. Major, M. C. Scharber, T. Sekitani, T. Someya, S. Bauer, N. S. Sariciftci, *Nat. Photonics.* **2013**, *7*, 811.
[22] H. Jinno, K. Fukuda, X. Xu, S. Park, Y. Suzuki, M. Koizumi, T. Yokota, I. Osaka, K. Takimiya, T. Someya, *Nat. Energy.* **2017**, *2*, 780.
[23] P. Jiang, J. Miao, X. Cao, H. Xia, K. Pan, T. Hua, X. Lv, Z. Huang, Y. Zou, C. Yang, *Adv. Mater.* **2022**, *34*, 2106954.
[24] H. Zhou, S. J. Han, A. K. Harit, D. H. Kim, D. Y. Kim, Y. S. Choi, H. Kwon, K. N. Kim, G. T. Go, H. J. Yun, B. H. Hong, M. C. Suh, S. Y. Ryu, H. Y. Woo, T. W. Lee, *Adv. Mater.* **2022**, *34*, 2203040.
[25] S. Chang, J. H. Koo, J. Yoo, M. S. Kim, M. K. Choi, D. H. Kim, Y. M. Song, *Chem. Rev.* **2024**, *124*, 768.
[26] Y. Zheng, S. Zhang, J. B. H. Tok, Z. Bao, *J. Am. Chem. Soc.* **2022**, *144*, 4699.
[27] X. Zhang, F. Wang, *APL Mater.* **2021**, *9*, 030701.
[28] H. Zhou, J.-W. Park, *Thin Solid Films.* **2016**, *619*, 281.
[29] R. E. Triambulo, H.-G. Cheong, H. Zhou, G.-H. Lee, J.-W. Park, *Jpn. J. Appl. Phys.* **2014**, *53*, 05FB13.
[30] H. Zhou, J.-W. Park, *Org. Electron.* **2015**, *24*, 272.
[31] H. Zhou, J.-W. Park, *Phys. Status Solidi A.* **2015**, *212*, 414.
[32] M. Pawlaczyk, M. Lelonkiewicz, M. Wieczorowski, *Adv. Dermatol. Allergol.* **2013**, *30*, 302.
[33] Y. Kim, J. Zhu, B. Yeom, M. Di Prima, X. Su, J.-G. Kim, S. J. Yoo, C. Uher, N. A. Kotov, *Nature.* **2013**, *500*, 59.
[34] S. Nam, M. Song, D.-H. Kim, B. Cho, H. M. Lee, J.-D. Kwon, S.-G. Park, K.-S. Nam, Y. Jeong, S.-H. Kwon, Y. C. Park, S.-H. Jin, J.-W. Kang, S. Jo, C. S. Kim, *Sci. Rep.* **2014**, *4*, 4788.
[35] S. J. Han, H. Zhou, H. Kwon, S.-J. Woo, T.-W. Lee, *Adv. Funct. Mater.* **2023**, *33*, 2211150.
[36] J. Liang, L. Li, X. Niu, Z. Yu, Q. Pei, *Nat. Photonics.* **2013**, *7*, 817.
[37] J. Liang, L. Li, K. Tong, Z. Ren, W. Hu, X. Niu, Y. Chen, Q. Pei, *ACS Nano.* **2014**, *8*, 1590.
[38] B. Wang, A. Facchetti, *Adv. Mater.* **2019**, *31*, 1901408.
[39] Y. Lee, J. Y. Oh, W. Xu, O. Kim, T. R. Kim, J. Kang, Y. Kim, D. Son, J. B.-H. Tok, M. J. Park, Z. Bao, T.-W. Lee, *Sci. Adv.* **2018**, *4*, eaat7387.
[40] L. V. Kayser, D. J. Lipomi, *Adv. Mater.* **2018**, *0*, 1806133.
[41] U. Lang, E. Müller, N. Naujoks, J. Dual, *Adv. Funct. Mater.* **2009**, *19*, 1215.
[42] Y. Lee, H. Zhou, T.-W. Lee, *J. Mater. Chem. C.* **2018**, *6*, 3538.
[43] J. H. Lee, Y. R. Jeong, G. Lee, S. W. Jin, Y. H. Lee, S. Y. Hong, H. Park, J. W. Kim, S.-S. Lee, J. S. Ha, *ACS Appl. Mater. Interfaces.* **2018**, *10*, 28027.
[44] S. Scholz, D. Kondakov, B. Lüssem, K. Leo, *Chem. Rev.* **2015**, *115*, 8449.
[45] J. H. Lee, S. Lee, S. J. Yoo, K. H. Kim, J. J. Kim, *Adv. Funct. Mater.* **2014**, *24*, 4681.
[46] K. Walzer, B. Maennig, M. Pfeiffer, K. Leo, *Chem. Rev.* **2007**, *107*, 1233.
[47] X. Zhou, J. Blochwitz, M. Pfeiffer, A. Nollau, T. Fritz, K. Leo, *Adv. Funct. Mater.* **2001**, *11*, 310.
[48] J. Meyer, S. Hamwi, S. Schmale, T. Winkler, H.-H. Johannes, T. Riedl, W. Kowalsky, *J. Mater. Chem.* **2009**, *19*, 702.
[49] M. Kröger, S. Hamwi, J. Meyer, T. Riedl, W. Kowalsky, A. Kahn, *Appl. Phys. Lett.* **2009**, *95*, 123301.
[50] I. A. de Castro, R. S. Datta, J. Z. Ou, A. Castellanos-Gomez, S. Sriram, T. Daeneke, K. Kalantar-zadeh, *Adv. Mater.* **2017**, *29*, 1701619.
[51] S. Ahn, S.-H. Jeong, T.-H. Han, T.-W Lee, *Adv. Opt. Mater.* **2017**, *5*, 1600512.
[52] L. V. Kayser, D. J. Lipomi, *Adv. Mater.* **2019**, *31*, 1806133.
[53] J. H. Kim, J. W. Park, *Sci. Adv.* **2021**, *7*, eabd9715.
[54] N. Matsuhisa, S. Niu, S. J. K. O'Neill, J. Kang, Y. Ochiai, T. Katsumata, H.-C. Wu, M. Ashizawa, G.-J. N. Wang, D. Zhong, X. Wang, X. Gong, R. Ning, H. Gong, I. You, Y. Zheng, Z. Zhang, J. B. H. Tok, X. Chen, Z. Bao, *Nature.* **2021**, *600*, 246.
[55] T.-W. Lee, Y. Chung, O. Kwon, J.-J. Park, *Adv. Funct. Mater.* **2007**, *17*, 390.
[56] T.-H. Han, Y. Lee, M.-R. Choi, S.-H. Woo, S.-H. Bae, B. H. Hong, J.-H. Ahn, T.-W. Lee, *Nat. Photonics.* **2012**, *6*, 105.
[57] T.-H. Han, M.-R. Choi, S.-H. Woo, S.-Y. Min, C.-L. Lee, T.-W. Lee, *Adv. Mater.* **2012**, *24*, 1487.
[58] Y.-H. Kim, C. Wolf, H. Cho, S.-H. Jeong, T.-W. Lee, *Adv. Mater.* **2016**, *28*, 734.
[59] Y.-H. Kim, H. Cho, J. H. Heo, T.-S. Kim, N. Myoung, C.-L. Lee, S. H. Im, T.-W. Lee, *Adv. Mater.* **2015**, *27*, 1248.
[60] Y. Shirota, H. Kageyama, *Chem. Rev.* **2007**, *107*, 953.
[61] F. Wang, W. Sun, P. Liu, Z. Wang, J. Zhang, J. Wei, Y. Li, T. Hayat, A. Alsaedi, Z. Tan, *J. Phys. Chem. Lett.* **2019**, *10*, 960.
[62] Z. Zhang, W. Wang, Y. Jiang, Y.-X. Wang, Y. Wu, J.-C. Lai, S. Niu, C. Xu, C.-C. Shih, C. Wang, H. Yan, L. Galuska, N. Prine, H.-C. Wu, D. Zhong, G. Chen, N. Matsuhisa, Y. Zheng, Z. Yu, Y. Wang, R. Dauskardt, X. Gu, J. B. H. Tok, Z. Bao, *Nature.* **2022**, *603*, 624.
[63] S. E. Root, S. Savagatrup, A. D. Printz, D. Rodriquez, D. J. Lipomi, *Chem. Rev.* **2017**, *117*, 6467.
[64] E. J. Sawyer, A. V. Zaretski, A. D. Printz, N. V. de los Santos, A. Bautista-Gutierrez, D. J. Lipomi, *Extreme. Mech. Lett.* **2016**, *8*, 78.
[65] Q. Pei, G. Yu, C. Zhang, Y. Yang, A. J. Heeger, *Science.* **1995**, *269*, 1086.
[66] H. Gao, S. Chen, J. Liang, Q. Pei, *ACS Appl. Mater. Interfaces.* **2016**, *8*, 32504.
[67] Z. Yu, X. Niu, Z. Liu, Q. Pei, *Adv. Mater.* **2011**, *23*, 3989.
[68] J. Xu, S. Wang, G.-J. N. Wang, C. Zhu, S. Luo, L. Jin, X. Gu, S. Chen, V. R. Feig, J. W. F. To, S. Rondeau-Gagné, J. Park, B. C. Schroeder, C. Lu, J. Y. Oh, Y. Wang, Y.-H. Kim, H. Yan, R. Sinclair, D. Zhou, G. Xue, B. Murmann, C. Linder, W. Cai, J. B.-H. Tok, J. W. Chung, Z. Bao, *Science.* **2017**, *355*, 59.
[69] X. C. Li, L. Yao, W. Song, F. Liu, Q. Wang, J. Chen, Q. Xue, W. Y. Lai, *Angew. Chem., Int. Ed.* **2023**, *62*, 202213749.

[70] W. Liu, C. Zhang, R. Alessandri, B. T. Diroll, Y. Li, H. Liang, X. Fan, K. Wang, H. Cho, Y. Liu, Y. Dai, Q. Su, N. Li, S. Li, S. Wai, Q. Li, S. Shao, L. Wang, J. Xu, X. Zhang, D. V. Talapin, J. J. de Pablo, S. Wang, *Nat. Mater.* **2023**, *22*, 737.
[71] A. P. Kulkarni, C. J. Tonzola, A. Babel, S. A. Jenekhe, *Chem. Mater.* **2004**, *16*, 4556.
[72] J. Kido, T. Matsumoto, *Appl. Phys. Lett.* **1998**, *73*, 2866.
[73] K. Xie, J. Qiao, L. Duan, Y. Li, D. Zhang, G. Dong, L. Wang, Y. Qiu, *Appl. Phys. Lett.* **2008**, *93*, 183302.
[74] J.-S. Yeo, M. Kang, Y.-S. Jung, R. Kang, S.-H. Lee, Y.-J. Heo, S.-H. Jin, D.-Y. Kim, S.-I. Na, *Nano Energy.* **2016**, *21*, 26.
[75] J. Ren, K. Ning, H. Liu, Z. Zhu, W. Fan, L. Wang, X. Zhao, S. Yang, *ACS Appl. Energy. Mater.* **2021**, *4*, 4489.
[76] S. Ohisa, T. Kato, T. Takahashi, M. Suzuki, Y. Hayashi, T. Koganezawa, C. R. McNeill, T. Chiba, Y.-J. Pu, J. Kido, *ACS Appl. Mater. Interfaces.* **2018**, *10*, 17318.
[77] T. Sasaki, M. Hasegawa, K. Inagaki, H. Ito, K. Suzuki, T. Oono, K. Morii, T. Shimizu, H. Fukagawa, *Nat. Commun.* **2021**, *12*, 2706.
[78] M. Choi, Y. J. Park, B. K. Sharma, S.-R. Bae, S. Y. Kim, J.-H. Ahn, *Sci. Adv.* **2018**, *4*, eaas8721.
[79] J. Kim, H. J. Shim, J. Yang, M. K. Choi, D. C. Kim, J. Kim, T. Hyeon, D.-H. Kim, *Adv. Mater.* **2017**, *29*, 1700217.
[80] M. Mansoor, I. Haneef, S. Akhtar, A. De Luca, F. Udrea, *Sens. Actuators, A.* **2015**, *232*, 63.
[81] J. H. Koo, S. Jeong, H. J. Shim, D. Son, J. Kim, D. C. Kim, S. Choi, J.-I. Hong, D.-H. Kim, *ACS Nano.* **2017**, *11*, 10032.
[82] T. Yokota, P. Zalar, M. Kaltenbrunner, H. Jinno, N. Matsuhisa, H. Kitanosako, Y. Tachibana, W. Yukita, M. Koizumi, T. Someya, *Sci. Adv.* **2016**, *2*, 1501856.
[83] C. Wang, D. Hwang, Z. Yu, K. Takei, J. Park, T. Chen, B. Ma, A. Javey, *Nat. Mater.* **2013**, *12*, 899.
[84] N. Oh, B. H. Kim, S.-Y. Cho, S. Nam, S. P. Rogers, Y. Jiang, J. C. Flanagan, Y. Zhai, J.-H. Kim, J. Lee, Y. Yu, Y. K. Cho, G. Hur, J. Zhang, P. Trefonas, J. A. Rogers, M. Shim, *Science.* **2017**, *355*, 616.
[85] X. Shi, Y. Zuo, P. Zhai, J. Shen, Y. Yang, Z. Gao, M. Liao, J. Wu, J. Wang, X. Xu, Q. Tong, B. Zhang, B. Wang, X. Sun, L. Zhang, Q. Pei, D. Jin, P. Chen, H. Peng, *Nature.* **2021**, *591*, 240.
[86] C. W. Tang, S. A. VanSlyke, *Appl. Phys. Lett.* **1987**, *51*, 913.
[87] M. A. Baldo, S. Lamansky, P. E. Burrows, M. E. Thompson, S. R. Forrest, *Appl. Phys. Lett.* **1999**, *75*, 4.
[88] H. Uoyama, K. Goushi, K. Shizu, H. Nomura, C. Adachi, *Nature.* **2012**, *492*, 234.
[89] W. Hu, X. Niu, L. Li, S. Yun, Z. Yu, Q. Pei, *Nanotechnology.* **2012**, *23*, 344002.
[90] J. Kim, J. Park, U. Jeong, J. W. Park, *J. Appl. Polym. Sci.* **2016**, *133*, 43830.
[91] Y. Chen, R. S. Carmichael, T. B. Carmichael, *ACS Appl. Mater. Interfaces.* **2019**, *11*, 31210.
[92] Z. Zhuo, M. Ni, X. An, L. Bai, X. Liang, J. Yang, Y. Zheng, B. Liu, N. Sun, L. Sun, C. Wei, N. Yu, W. Chen, M. Li, M. Xu, J. Lin, W. Huang, *Adv. Mater.* **2023**, *35*, 2303923.
[93] Y. Liu, M. Zhu, J. Sun, W. Shi, Z. Zhao, X. Wei, X. Huang, Y. Guo, Y. Liu, *Adv. Mater.* **2022**, *34*, 2201844.
[94] M. W. Jeong, J. H. Ma, J. S. Shin, J. S. Kim, G. Ma, T. U. Nam, X. Gu, S. J. Kang, J. Y. Oh, *Sci. Adv.* **2023**, *9*, eadh1504.
[95] J.-H. Oh, J.-W. Park, *ACS Appl. Mater. Interfaces.* **2023**, *15*, 33784.
[96] L. Yin, K. N. Kim, J. Lv, F. Tehrani, M. Lin, Z. Lin, J.-M. Moon, J. Ma, J. Yu, S. Xu, J. Wang, *Nat. Commun.* **2021**, *12*, 1542.
[97] W. Seung, M. K. Gupta, K. Y. Lee, K.-S. Shin, J.-H. Lee, T. Y. Kim, S. Kim, J. Lin, J. H. Kim, S.-W. Kim, *ACS Nano.* **2015**, *9*, 3501.
[98] E. H. Kim, S. H. Cho, J. H. Lee, B. Jeong, R. H. Kim, S. Yu, T.-W. Lee, W. Shim, C. Park, *Nat. Commun.* **2017**, *8*, 14964.
[99] H. Jinno, T. Yokota, M. Koizumi, W. Yukita, M. Saito, I. Osaka, K. Fukuda, T. Someya, *Nat. Commun.* **2021**, *12*, 2234.
[100] H. Seung, C. Choi, D. C. Kim, J. S. Kim, J. H. Kim, J. Kim, S. I. Park, J. A. Lim, J. Yang, M. K. Choi, T. Hyeon, D.-H Kim, *Sci. Adv.* **2022**, *8*, eabq3101.